Towards Modelling the Formation of Ore Bodies : initial results dealing with the fluid mechanical aspects of magma chamber convection

A thesis submitted to

Rhodes University

in fulfilment of the requirements

for the degree of

Master of Science

André Erasmus Botha

January 1999

Abstract

This thesis forms part of a larger effort which aims to establish the means of assessing the fluid mechanical behaviour of *magma* [1] as it cools inside a magma chamber surrounded by porous *country rock*. The reason for doing so is to advance the understanding of some types of mineral deposits; for example, the *Platinum Group Elements* (PGEs). The magma is modelled with the governing equations for a single-phase incompressible Newtonian fluid with variable viscosity and density. In this thesis, thermal conductivity and specific heat are approximated as constants and the country rock is treated as a conducting solid so as to save on computational time in the initial phases of the project. A basic review of the relevant literature is presented as background material and three basic models of magma chambers are discussed: crystal settling, compositional convection and double diffusive convection. The results presented in this thesis are from finite element calculations by a commercial computer code: ANSYS 5.4. This code has been employed in industry for over 26 years and has a long and successful benchmark history. In this context, finite element methods that are applicable to the code are discussed in chapter 5. In chapter 6, results that were obtained in the course of this research are presented. The thesis concludes with an indication of the possible geological significance of the results and various refinements that should be made to future models.

[1] Italicised terms are defined in the glossary of Appendix A.

Acknowledgements

I am extremely grateful for the generous financial and academic support which I have received from Professors Alan Rice and Fabio Frescura. The Department of Physics and Electronics kindly granted me the use of their LaTeX2e facilities and supplied me with an office, additional financial support, and very helpful course-work on fluid mechanics during my studies at Rhodes. The Department of Geology has provided much appreciated help in mastering the basics of geology. I also had the privilege of having many constructive discussions with various members of staff who were always enthusiastic about the project. The Departments of Computer Science, Pharmaceutical Sciences and Chemistry were also instrumental in providing adequate computational hardware to perform the calculations.

Contents

List of Tables

List of Figures

Chapter 1

Introduction

1.1 The importance of igneous intrusions in ore body formation

One of the main motivations for studying *igneous intrusions* [1] is economic. *Ore deposits* are closely linked with both *silicic* and *mafic* igneous intrusions. Mafic intrusions, in particular those that are layered, can in some situations yield ore bodies which contain Platinum Group Elements (PGEs).

Furthermore, in favourable terranes, namely in highly jointed, permeable rocks, igneous intrusions act as "heat engines" that provide the energy necessary to promote long lived convective circulation of any mobile water in the *country rock* surrounding the magma chamber. Most often the mobile water surrounding the intrusion is well above its critical point and is thus

[1] The fist occurrence of all words that are defined in the glossary of Appendix A are italicised.

even more able to dissolve minerals that are contained in the country rock to form a so-called hydrothermal solution (Barnes, 1979). Upon cooling, the dissolved load will precipitate mineral deposits.

Other deposits that are closely linked with igneous intrusions are porphyry deposits. The most important porphyry deposits are those of copper-bearing sulphides, yielding, in 1979, more than half of the world's annual copper production (Gustafson, 1979). Commonly, molybdenum, gold, silver, lead and zinc are also extracted as byproducts of copper mining. Molybdenum, tungsten and tin are the primary products of porphyry deposits.

In the above case of hydrothermal deposits, the fractures in which the mineralisation occurs are believed to have formed late in the emplacement history of the associated igneous intrusion. During the cooling history, the process of fractional crystallisation occurs within the magma chamber. This important process is responsible for *layering* in igneous intrusions. Layering is thought to be closely linked to natural concentrations of valuable minerals. For example, the Bushveld Complex (South Africa), one such layered intrusion, is the largest known repository of PGMs in the world. Estimates for 1995 indicate that 55.7% of the world's PGMs that have been mined came from the mafic rocks of the Bushveld (Hess, 1996).

There is no reason to believe that the mineralisation of the Bushveld is unique. Most (but not all) of the other layered complexes listed in Table 1.1 contain substantial amounts of valuable *mineral deposits.* In some cases however, the *reserve base* is not of economic value. This fact is related to the size (thickness) of the complex : only thick units yield payable reserves (ore bodies) (Rice, 1997b).

Table 1.1: Some of the layered complexes that are of interest to this work are found all over the world (Maaloe, 1985).

Complex	Area/[km^2]
Bushveld, South Africa	66 000
Dufek, Antarctica	50 000
Duluth, United States	4 700
Stillwater, United States	4 400
Muskox, Canada	3 500
Great Dike, Zimbabwe	3 300
Sudbury, Canada	1 300
Skaergaard, Greenland	100

1.2 Present models of igneous intrusions

At the time of this writing (December 1997), there exist several competing models of igneous intrusions. Each of these is based on only one or two dominant physical processes and neglects a large number of interrelated processes that are also thought to occur. The rationale behind this is that the neglected processes are thought not to contribute significantly to the phenomena of interest. This neglect is not always physically justified but has in the past been admitted because of the lack of computational power. With recent advances in computational devices and techniques, models of large igneous intrusions, which require the simultaneous solution of the equations governing the convection inside the magma chamber as well as those for the associated hydrothermal flow in the porous country rock surrounding the chamber, are now tractable. Table 1.2 summarises five prominent models of igneous intrusions together with the main problems associated with each

model in recent literature.

These five models have been named according to the main physical process on which they are based, since each model assumes that a single physical process dominates the formation of layering. The first three of these models will be discussed in more detail in Chapter 2.

The notion of crystal settling attributes the evolution of magmas to the settling out of crystals from the melt as the magma cools. However, a proportion of recent literature indicates that the crystals will be convected along with most melts rather than settle. Typically, magma chambers of depth greater than some tens of metres undergo vigorous convection wherein crystals of even substantial size (up to about 1cm) may have difficulty settling (Rice, 1993).

Compositional convection, as opposed to thermal convection, is due to density variations that occur in the melt as a result of compositional changes of the melt during crystallisation. These compositional inhomogeneities arise because magmas are complicated *eutectic systems*. Crystals that form have a higher density than the melt from which they crystallise. If crystals are thus removed from the melt, the density of the melt will initially decrease and this may provide the buoyancy instability necessary for compositional convection. However, there is evidence that a percentage of crystals is retained in the melt (Rice and Eales, 1995). Calculations then show that the effective (bulk) density of the magma (which includes its crystal load) overwhelms the effect of compositional change of the melt (Rice and Eales, 1995).

Double diffusive convection could occur in magma chambers because temperature and chemical composition may both vary with the depth of the

Table 1.2: Five of the main models of layered intrusions classified according to a dominant underlying physical process. Entries in the right hand column lists the main problems with each of the models described in the corresponding row of the centre column.

Process	Description	Problem
Crystal Settling	convection not important as crystals sink down through the less dense uncrystallised melt (Weinstein et al., 1988) (Marsh, 1989)	"By the end of the 1970s the classical model of crystal settling was unsatisfactory"(Martin, 1989) Also see Rice (1995).
Compositional Convection	convection is mainly due to density variations caused by compositional changes rather than thermal changes (Sparks and Huppert, 1984)	even a small % of retained crystals in the melt would negate the effects of compositional variations in density (Rice and Eales, 1995)
Double Diffusive Convection	convection in chamber due to variations in temperature and chemical composition (Rice, 1981)	crystal retention will alter this mechanism as discussed above (Rice and Eales, 1995)
Two-phase Natural Convection	convection in chamber is strongly dependent on the suspended crystal load (Rudman, 1992)	no major objections but models are incomplete since they use constant viscosity and are only in two dimensions
Multiple Injections	chamber gets replenished with parent magma several times during cooling history (Huppert et al., 1982)	same as for two-phase natural convection Also see Rice (1997a).
Bottom Crystal Growth	bottom crystallisation involving Rayleigh fractionation or diffusion control (McCarthy et al., 1985) (See also Jackson 1961)	most compatible with Cr abundance profiles but the apparent inhomogeneity that occurs in the magma is not explained

chamber. Temperature and chemical composition diffuse at different rates which often causes the formation of many separate horizontally convecting layers in the fluid. Work leading up to this thesis assumes that no crystals are retained in the melt. Furthermore, as noted by Rice (1982), many researchers (for example Sparks and Huppert, 1982) do not incorporate dynamic similitude into their experimental studies that are supposed to replicate magma chambers. The computational modelling by Hansen (1987) investigates the effect of the chamber aspect ratio and boundary conditions but neglects the important effects of viscosity variations and time evolution; only the steady state Navier-Stokes equations were solved using constant viscosity.

The computer modelling work of Spera, Yuen and Kirschvink (1982) attempts to model the thermal boundary layer convection in silicic magma chambers. In contrast to the work done by Hansen (1987); Spera, Yuen and Kirschvink (1982) allow for what they term a non-Arrhenius [2] viscosity variation with temperature. The equation they use has the form

$$\mu = \mu_\infty \exp\left[-a\left(T_\infty - T_0\right)\right] \tag{1.1}$$

where μ_∞ is the apparent viscosity of the melt at the liquidus temperature, denoted by T_∞. Using this equation, the authors account for the effect of crystal content and temperature on the magma viscosity, μ. Even so, their work is limited to relatively low Rayleigh numbers ($Ra < 10^4$) and therefore has limited applicability to real situations. It is shown in Appendix D, that a typical magma chamber can convect with an initial Rayleigh number of 10^{12}. This has been known for many years (Rice, 1981; Bartlett, 1969; Shaw, 1965).

[2] They are in fact making use of the well known Frank-Kamenetskii approximation to the Arrhenius law.

The work of Spera, Yuen and Kirschvink (1982) is also limited to two dimensions only. Preliminary calculations from ANSYS 5.4 have indicated radical differences between convection in equivalent two and three-dimensional chambers. For example, in a three-dimensional cylinder, upward spiralling convection can occur early in the cooling history at Rayleigh numbers as low as 10^7. An example of this is shown by the the velocity vectors of a rhyolitic magma convecting inside a cylindrical magma chamber; Figure 1.1. This three-dimensional spiralling behaviour of the magma in the cylinder is not observed in an equivalent two-dimensional model consisting of two-dimensional convection in a rectangle with the same dimensions as a vertical cross section through the cylinder shown. For further discussion of the chamber shown in Figure 1.1 consult Botha et al. (1996a), (1996b).

There have been attempts (Rudman, 1996) at modelling two-phase natural convection in magma, assuming the magma to be a Newtonian fluid with a suspended solid crystal load. An initial homogeneous distribution of crystals within the melt is assumed and a volume averaging technique is used in which averaging is performed over both phases simultaneously. This leads to equations that describe heat and mass transport in the mixture rather than transport in each phase separately. Rudman's (1996) calculations indicate that the crystal distribution changes to being heterogeneous, but his models are not coupled to the associated hydrothermal activity in surrounding porous country rock.

Multiple injection models require that the magma chamber be replenished with influxes of new parental magma of different compositions at varying intervals during the cooling history of the chamber. These models are invoked to explain certain features of layering based on geological observations but,

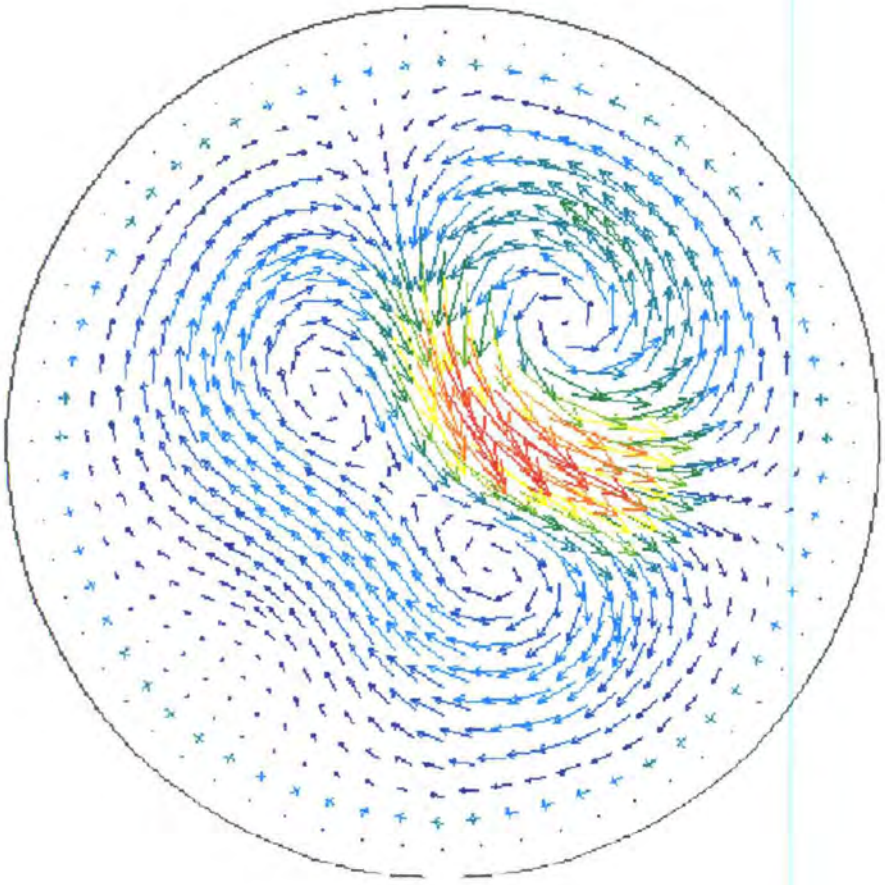

Figure 1.1: Velocity vectors as seen from the top of a cylindrical magma chamber when it is standing upright, gravity pointing into the page. The velocity vectors are also colour coded from red, the maximum velocity, through blue, the minimum velocity. The warmer magma in the interior of the cylinder is spiralling (swirling) upwards as the cooler magma sinks down along the sides of the cylinder. This cylinder is 1km in diameter and 500m deep, $Ra \approx 10^8$. See Botha et al. (1996a), (1996b).

the theory is essentially self contained in that it has no physical basis, i.e. injections are invoked at the required frequency that accounts for the layering. The injections themselves, are not explained in terms of some underlying physical mechanism.

1.3 Main objective of this thesis

This thesis should be viewed as a small component of a much larger project which aims at devising a computational model for the formation of ore deposits associated with igneous intrusions and surroundings. The major hypothesis made is that the processes of interest are governed by the equations of fluid mechanics and other known physical laws. Although, as a first phase of the project, very silicic (high viscosity) magma chambers which show very little layering were treated, future models will incorporate all types of igneous intrusions, whether they are layered or not. Furthermore, geological units of any size and shape can be modelled by the finite element approach taken in this project.

The ultimate objective of the whole project is the construction of a computational model to which a client may bring initial conditions of a geological unit of interest and receive, from the model, the anticipated distributions of mineralisation derived from the equations describing solidification and/or porous media flow and chemical transport.

1.4 Outline of thesis

The material in this thesis is organised as follows.

Chapter 2, describes the physical situation that is to be modelled. Specifically, some petrological evidence that could help explain the genesis of layered intrusions is investigated. The main purpose of this is to show that the models of chapter 6 are consistent with the current geological views on the formation of igneous intrusions. Also presented, is a description which elaborates on three of the five prominent fluid mechanical models of magma chambers: crystal settling, compositional convection and double diffusive convection. These models have been particularly useful in the development of this work and comparison shows that the modelling work in this thesis avoids many of the difficulties that are presently associated with these standard models.

Chapter 3, considers the physical properties of magmas. Here the present understanding of the physical characteristics of magma is reviewed. Where it is of importance to this project, the relation between the physical properties of the magma and its composition is also investigated. At present, this is only of academic interest since higher accuracy in the physical parameters is not necessary for the preliminary models in chapter 6. Furthermore, models of actual geological units (like the Bushveld Complex) will in future be based on the adequate experimental data that is available.

Chapter 4 explores some fluid mechanical aspects of the project which again are not necessarily directly related to the modelling process. This chapter is included mainly as an illustration of the theory which had to be covered to provide necessary background before actual modelling could begin. The project as a whole draws heavily on theory from a wide range of disciplines:

fluid mechanics, geology, chemistry, computational physics and computer science. Elements from all these disciplines had to be assimilated during the course of this research. In this respect, chapter 4 is of academic interest, although its main contribution is in providing a means to establish benchmark calculations for the preliminary finite cylinder models. This is in fact one of the main reasons for doing these preliminary calculations with cylinders. It is important to have these calculations as a reference for comparison to real magma chamber calculations, the accuracy of which cannot easily be ascertained from first principles or analytic solutions. In this respect the method used at the end of chapter 4, to benchmark the calculations for cylinders using Bessel functions, is only one instance of a fundamental technique employed frequently in finite element modelling.

Chapter 5 deals with the basic method of finite elements and the solution of the governing differential equations that were discussed in chapter 3. A more extensive discussion of finite element technique would be beyond the scope of this thesis and is also unnecessary: the comparison of predictions from the code with actual known analytic solutions is widely accepted in the field as the best method for ascertaining the validity of solutions. The remaining task of developing better finite elements techniques for the problem at hand is highly specialised and is typically undertaken by large teams of highly skilled experts.

Chapter 6 describes some basic models of a igneous intrusions. All the assumptions are listed and the results from these preliminary models are presented so as to give the reader a better understanding of the type of results that more sophisticated models will be able to predict.

Chapter 7 concludes by suggesting likely improvements that are soon to be

made in future models, as more sophisticated computer hardware becomes available. The geological significance of each of the preliminary models presented in this thesis is also discussed.

Chapter 2

Current Models of Layered Intrusions

2.1 Introduction

Igneous Petrology is the study of the composition, structure, and origin of rocks that form by the solidification (freezing) of a magma. In particular, one of the major branches of igneous petrology is the study of igneous intrusions which are of economic importance because of their associated mineralisation. Usually the mineralisation occurs either because of hydrothermal activity in the surrounding porous country rock or because of fractional differentiation that occurs within the actual magma chamber. In both cases the minerals form by chemical reactions. The formation of minerals is thus determined firstly by the composition of the magma available and secondly by the physical conditions such as temperature and pressure that govern the kinetics whereby they are formed. It is important to note that both these factors

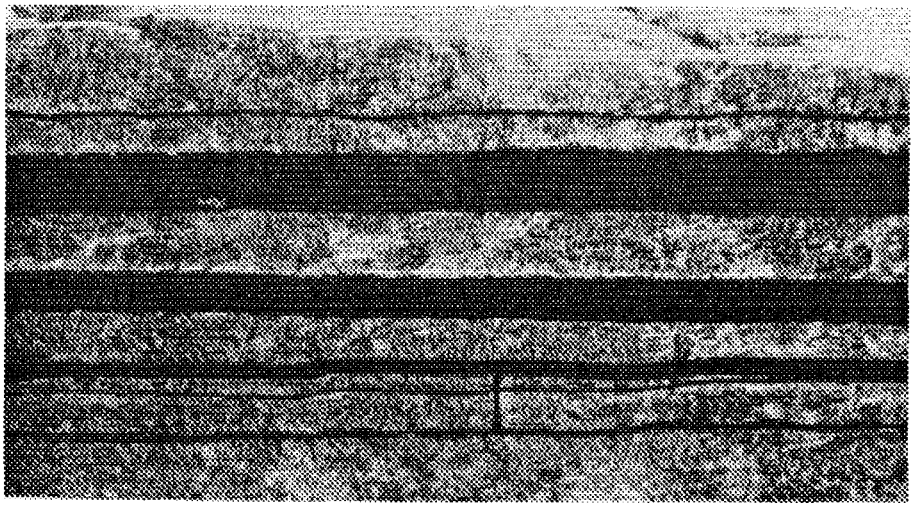

Figure 2.1: Chromite seams (dark) within anorthosite, Bushveld Complex, South Africa. These seams can range in thickness from only a millimetre up to metres. They can have lengths of several kilometres and are frequently bifurcated (see for example the right hand side of the second chromite seam from the bottom). This picture is from Wager and Brown (1967), page 362.

are affected indirectly by the country rock that surrounds the chamber. For example, country rock could be melted by the intrusion and assimilated into the chamber thus affecting the composition of the magma. As discussed later, the country rock also plays an important role in the rate of heat loss from the chamber. Figure 2.1 shows a typical example of igneous layering. Chromitite layers such as these are almost monomineralic and hence of considerable economic importance.

In order to predict where and what types of minerals form from a given magma, the physical conditions in and around the chamber, during and after its emplacement, must be known. This is the main reason why quantitative models of layered intrusions are so important.

Perhaps the most important example of a layered intrusion is the Bushveld Complex. This complex is situated in a region, north of Pretoria, that covers approximately 182 000 km^2 of the Kaapvaal Craton, South Africa. Its formation is commonly believed to have taken place in three main stages which occurred over 2×10^9 years ago. These three distinct periods [1] of magmatic activity are believed to be responsible for the deposition of *igneous rocks* which are now typically classified into three main corresponding divisions. It is worth noting however that there are workers who believe, with good reason, that the Lower Zone of the Bushveld is actually the base of the complex. Either way, it is not of critical importance in the present work and is therefore merely noted as a passing point of interest.

- Bushveld Granites - granitic rocks that form the top and periphery of the complex
- Layered Series - mafic and ultramafic rocks up to 9000 m thick in places forming the middle of the complex. [2]
- Marginal Zone - alternating laminated sheets of dunite and pyroxenite which form the base of the complex [3]

A simplified map of the surface exposures of the Rustenburg Layered Series (RLS) is shown in Figure 2.2. Of the above three classes, the Layered Series

[1] At present it is typically thought that these three distinct periods of magmatic activity were actually coeval, i.e., contemporary.

[2] In more recent literature the Layered Series is called the Rustenburg Layered Suite (RLS). This term typically includes the Marginal Zone (see next footnote) but the terminology in the literature is not always consistent.

[3] The Marginal Zone is sometimes included as a lower part of the Layered Series in more recent classifications.

is the only one of present economic importance. It is typically divided into five zones as shown in Figure 2.3.

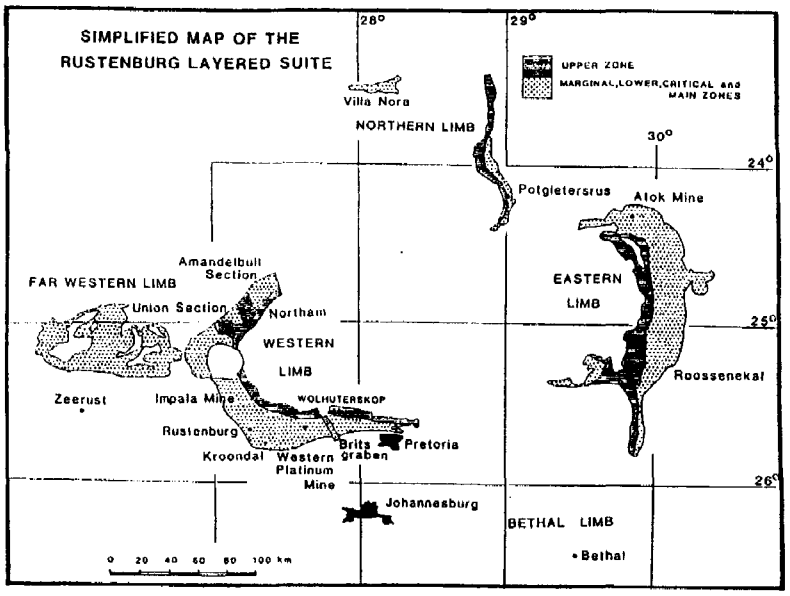

Figure 2.2: A simplified map showing the surface exposures of the Rustenburg Layered Suite (RLS) of the Bushveld Complex which underlies most of the region shown in this map. From Eales et al. (1993).

The emplacement of the Layered Series is currently still a controversial topic in the literature. Many authors disagree completely while some have views that are at least partially compatible with those held by others. Some of the main proposals are outlined here.

The formation of the whole Layered Series, could have, on the one extreme, formed by one single pulse, or may have involved only three different lineages or pulses of parental magma. The first pulse could be parental to the Lower and Critical Zones, the second to the Lower Main Zone and the third to

the Upper Main Zone and the Upper zone. This multi-pulse mechanism is sought to explain observed $^{87}Sr/^{86}Sr$ distributions (Sharpe, 1985). On the other hand it has been proposed (Eales et al., 1993) that each layer (some only on the order of millimetres) could represent a separate pulse. There are many variations on the above ideas depending on the author one reads.

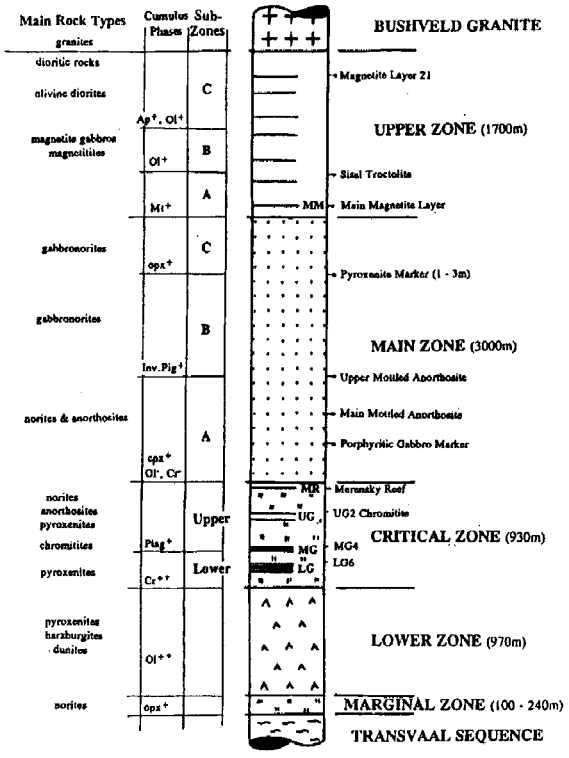

Figure 2.3: Geological column of the Layered series of the Bushveld Complex from Eales et al. (1993).

The chromite layers and the principle platiniferous layers of the Layered Series are confined to the Critical zone. This zone is of overwhelming economic importance and its genesis is typically debated qualitatively (as in the above discussion) in terms of

- fractional crystallisation from one or more parent magma
- successive injection of magma.

Many other mechanisms have been proposed to explain the emplacement and subsequent evolution of layered intrusions that are similar to Layered series in the Bushveld. Even though most people agree that layered intrusions form by fractional crystallisation, there is currently no single physical model that explains all the observed features associated with layered intrusions. Many of the existing models do however predict some features of layered intrusions which are consistent with the observed data. They thus provide an important starting point for the development of more successful models and must therefore be examined here.

2.2 Crystal Settling

Crystal Settling is the process whereby crystals that form inside a magma chamber are believed to sink down, under the influence of gravity, through the remaining uncrystallised melt. The idea of Crystal Settling was introduced to Geology by Charles Darwin. Over 150 years ago he described the settling of crystals in a basaltic lava flow on the Galapagos Islands (Darwin, 1844).

In 1914 Norman Bowen of the Carnegie Institution in Washington claimed to have demonstrated the process of crystal settling in the laboratory (Bowen, 1915). The experiment consisted of placing a melt in a platinum crucible. The melt was left for a sufficiently long time to develop crystals. The crystals were then prevented from further growth by quenching the melt, thus embedding the crystals in a glass. According to Bowen, thin sections of this

glass taken at various positions along the centre line of the crucible revealed that a larger proportion of crystals were found at the bottom of the crucible than at the top.

The work of Wager and Brown (1967) on the Skaergaard Intrusion in Greenland was also particularly influential in establishing the idea of crystal settling. Towards end of 1960 people were using the terms crystal settling and fractional crystallisation as synonyms.

It was not until the 1970s that a number of awkward features of the theory of crystal settling were pointed out by Alexander McBirney, who led expeditions to revisit the Skaergaard Intrusion (McBirney and Noyes, 1979), and Ian Campbell, who examined the Jimberlana Intrusion in Western Australia (Campbell, 1978). Their objections are as follows:

- Layering sometimes occurred in steeply sloping surfaces. Crystal settling can only account for the formation of horizontal layers.
- Sometimes the heaviest minerals were at the top and the lighter minerals were at the base. This is opposite to the predictions of the crystal settling theory.
- Often the crystals that have settled are less dense than the magma through which they are presumed to have sunk. This is in conflict with the basic laws of physics.
- Calculations that take into account the finite yield strength of magma indicate that crystals would have to be the size of a house before they will be able to overcome the yield strength of the magma in order to sink.

- Thermodynamic considerations show that crystals are more likely to grow against the pre-existing rocks on the margins of the magma chamber rather than forming from the liquid in the interior of the chamber.

Bowen's original paper has been criticised because he did not mention crystals which formed nearer the middle of the crucible were much larger than those close to the bottom (Rice, 1981). This can be seen in Figure 2.4. The total volume fraction of crystals in fact appears equal throughout the whole crucible [4]

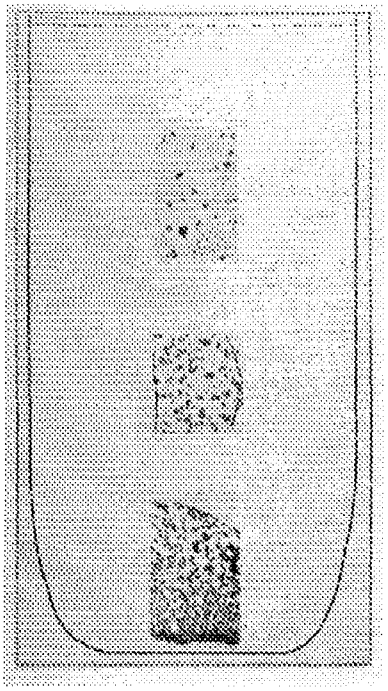

Figure 2.4: Illustration of N.L. Bowen's experiment on the sinking of diopside crystals in a melt. The relative positions in the crucible of three thin sections cut from the quenched melt are shown. The abundance of the diopside crystals increases downwards but the grain-size decreases. From Bowen (1915), page 178.

Since the sides of the chamber cooled faster than the central region, the crystals nearer the sides did not have as much time to grow as those that were closer to the middle. Experiments similar to Bowen's revealed that the

[4]There are apparently no point counts available to establish actual volume fractions (the thin sections have likely long disappeared, making it impossible to do so).

gradation in crystal size toward the sides of the crucible is the same as that toward the bottom. Thus, to quote Rice (1981): "This is not to dismiss crystal settling ... but to point out that ... more than one interpretation of Bowen's pot (a case of quenching rather than crystal settling) can be entertained ..."

Huppert et al. (1984) have calculated that the convective velocities are orders of magnitude greater than the settling velocities of typical crystals. Thus in a typical magma chamber the crystals that form in the interior of the melt would be transported by the convection currents in the direction of the magma flow. They would therefore have little opportunity to settle.

Recently, more quantitative approaches to the problem have led to the conclusion that crystal settling is not physically plausible. See, for example, Huppert and Turner (1991) who argue against the idea of crystal settling put forward in Weinstein et al. (1988) and Marsh (1989). The section entitled "Time to settle the crystal theory" in Martin (1989) summarises some obvious problems with the theory. It concludes as follows: "By the end of the 1970s the classical model of crystal settling was unsatisfactory. The time was ripe for new ideas." In short, a number of recent workers hold that crystal settling is not significant in a typical magma chamber and cannot produce fractional crystallisation simply because, as Rudman (1992) claims, " ... it does not typically occur". See also Appendix C for details on the calculation which shows that crystals cannot typically settle.

2.2.1 Compositional convection

Compositional convection occurs when chemical changes in the magma, because of crystallisation, cause density changes that make the magma convect. According to this view, crystals do not form in the interior of the chamber but form mainly on the pre-existing rock on the margins of the chamber. Thus crystals form within a cooler boundary layer that surrounds the hot parent magma. Because crystals have formed on the wall, the boundary layer, next to the wall, changes its chemical composition. Turner (1980) points out that the depleted magma in the boundary layer should in general be less dense than the magma in the interior of the chamber; in spite of the boundary layer being cooler. Thus the magma along the sides of the chamber is more buoyant and will rise. Crystallisation on the floor of the chamber also leaves behind lighter magma which again provides the instability necessary for compositional convection. As the depleted magma rises it mixes into the main body of magma which therefore slowly changes its composition. This is one manifestation of fractional crystallisation.

Although some researchers claim partial success with this theory (Weinstein et al., 1988), important issues are still not resolved. For example, density variations that include the effect of the suspended load, could in fact dominate the compositional density changes (Rice and Eales, 1995).

2.2.2 Double-diffusive convection

Double-diffusive convection can occur in fluids whose density is a function of temperature and composition, when the effect of temperature and com-

position on the density of the fluid propagate through the fluid at different rates. A classical example of a system which undergoes double-diffusive convection is a solution of salt in water. The density of the water increases as a result of either increasing the concentration of salt, or removing heat from the solution.

The rate at which heat diffuses through the solution is orders of magnitude greater than that of the solvated salt ions. If the case is considered where cold fresh water is in contact with a warmer saline solution, two convective modes arise. See for instance Turner (1973).

- **Diffusive mode:** the cold fresh water over-lies a layer of warmer salty water. This situation is possible if the salinity of the warmer water is high enough to make it more dense than the overlying cold water. Both heat and solvated salt ions will tend to diffuse into the upper layer. However since the heat diffuses much faster than salinity, the net effect of the combined diffusion will be that the lower part of the upper layer rises while the upper part of the lower layer sinks (as it cools). The diffusive mode can give rise to the formation of many layers which can then telescope one into another as a form of rollover.

- **Finger mode:** the hot salty water lies above the denser, cold, fresh water. Again, the initial distribution of density is stable since, if the salinity of the top solution is not excessively high, the saline solution can be brought to a temperature at which its density is lower than that of the fresh water below. Now, if the system is left to stand, the heat from the top layer diffuses downwards causing the cold underlying fresh water to become less dense than the saline layer above. Tall narrow vertical structures known as "fingers" form at the interface between

the two layers. Warmed fresh water rises in fingers from the top of the lower layer into the upper layer. Fingers of heavier salty water descend. These fingers form because heat diffuses more rapidly than the salt ions. Two separate convection layers occur, one above and one below the interface. As in the diffusive case, these layers also typically multiply into a many layered system, every other layer driven by finger convection. The well know salt fountain is a manifestation of this effect.

In magmas, double-diffusive convection is thought to occur as a result of compositional changes which are due to crystallisation, assimilation of country rock or injection of a new pulse of magma. The magma must however exhibit a compositional change in the vertical direction, either continuous or discontinuous (Turner, 1980; Chen and Turner, 1980; Huppert and Turner, 1991). This last requirement is frequently debated in the literature. One of the main mechanisms proposed for obtaining the initial conditions necessary for the occurrence of double-diffusive convection is similar to that used in the theory of compositional convection where the assumption is made that no crystals are retained in the melt. Another mechanism (Rice, 1997a; Rice and Eales, 1995) proposes that the necessary compositional variations in the vertical can be due to the retention of crystals in the melt. As yet there is no consensus in the literature on this topic.

2.3 Conclusion

Some complications in the modelling of magma chambers are:

- the large number of coupled physical degrees of freedom driving the

flow inside and around the chamber where hydrothermal groundwater may exist

- the complex and often unknown or changing geometries that a chamber could have assumed during its history. [5]
- variation in the physical properties of the magma (better and more extensive data would improve modelling efforts)
- the non-Newtonian behaviour of the magma below its liquidus temperature and the effects of a possible crystal load
- the effect of crystals in the melt on the properties of the flow, making it effectively a two-phase flow
- the heating of the surrounding country rock and the removal of heat by circulating ground water in the porous country rock
- the question whether a magma chamber may successfully be treated as a closed system, i.e. one in which the magma is emplaced in a single, relatively rapid injection and then crystallises without loss, or whether it should rather be treated as an open system, i.e. one in which the magma is emplaced in several pulses separated by time intervals lengthy enough to permit significant cooling and the formation of cumulates with the possibility of intermittent leakage.

With the exception of the last problem, all the other problems above can in principle be solved by increasing the complexity of current numerical models such as those discussed in chapter 6. To throw light on the last problem, pulses can be induced in the numerical modelling, the results of which, can

[5] Computational modelling of freezing chambers has thrown some light on this.

then be compared with the geological arguments for and against multiple pulses.

Most current models of magma convection incorporate only one or two of the above physical influences at a time. In order to improve on previous work, future modellers will have to incorporate many more of the above physical influences into their models. The work in this thesis, and also the project as a whole, is an attempt at initiating such a move. With recent advances in computer technology, this goal is no longer impossible. Computational methods and hardware have now advanced to the stage where quantitative numerical models of magma chamber convection can be made at relatively low cost and without any of the simplifying assumptions that have been necessary in the past.

Chapter 3

Physical Properties of Magmas

3.1 Introduction

All magmas can be classed as *polymers*. Much of what is known about the physical behaviour of magmas can be explained in terms of the properties of the silicon and oxygen ions which are usually the most abundant components of igneous rocks. Melts that are very rich in silica are characterised by molecular tetrahedra of silicon which are linked in 3-dimensional networks by oxygen atoms, most of which are shared by two or more tetrahedra. Other cations can enter the melt in limited amounts as independent ions occupying the positions between the tetrahedra. When they do so, they modify the basic structural framework and alter its physical properties. In this way Si, and to a lesser degree Al, act as so called "framework-forming" atoms. Typically Mg, Ca, Fe, Na, and most other metals occupy positions within the basic framework structure and are thus referred to as "framework modifiers". These atoms can be accommodated in amounts up to about 20 cation percent

before the basic framework begins to break down into smaller geometric units. When more than than 66 % of the cations are framework modifiers, each Si atom forms a separate tetrahedron that is not linked directly to another. These melts are called orthosilicates.

There have been many attempts to quantify the physical properties of magma mathematically based on the composition of the magma (Bottinga and Weill, 1972; McBirney and Murase, 1984). Typically these models are derived by performing multi-variable regression on physical property data of melts with various compositions. Usually the results are only applicable within a small range of composition because of the previously mentioned fundamental structural changes in the melt. An additional complication is that the physical properties of a given melt will change with time as crystallisation takes place, even when all other physical parameters are held constant. For example, a basaltic magma at 1100°C which is left undisturbed for five hours can increase its viscosity from 10^3 Pa·s to 10^5 Pa·s over this period (Williams and McBirney, 1979).

It is primarily because of the difficulties mentioned above that no attempt will be made to formulate a theoretical model for the physical properties of magmas. This would be beyond the scope of this thesis. Furthermore, viscosity data for magmas typically has uncertainties of up to 20 % and it is very difficult to make more accurate viscosity measurements. To obtain sufficient data with which to compare theoretical models would require funding beyond the scope of this entire project. It is in any case not necessary in this preliminary stage of the project as the present data that is available is adequate for the exploration of important issues that have not been resolved. Even so, in order to give the reader a basic intuitive understanding of the

functions used to model the physical properties of magma, there follows a brief description of the main factors that influence these properties.

3.2 Viscosity

For Newtonian liquids the stress, τ, is proportional to the velocity gradient. This is shown in Figure 3.1 for a liquid flowing only in the x direction.

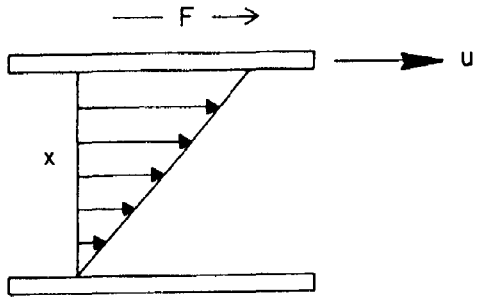

Figure 3.1: The definition of the dynamic viscosity, μ, in terms of two thin plates, each of area A. The upper plate is acted on by a shear stress $\tau = \frac{F}{A}$ and moves to the right with velocity u. From Schowalter (1978)

The strain rate is given by the velocity gradient du/dx and is related to the shear stress by the dynamic viscosity μ in the relation

$$\tau = \frac{F}{A} = \mu\left(\frac{du}{dx}\right) \tag{3.1}$$

A generalisation of equation (3.1) to 3-dimensional flows is possible but this is not required at present (Currie, 1993). For Newtonian fluids, the viscosity is independent of the stress, but not for non-Newtonian fluids. Below their liquidus temperatures, magmas are not simple Newtonian fluids and are observed to display a variety of non-Newtonian behaviour including Bingham,

dilatant, pseudoplastic and even thixotropic behaviour (Maaloe, 1985). Since the viscosity of magma will be modelled from experimental data that includes viscosities below the liquidus, where the non-Newtonian behaviour becomes important, non-Newtonian behaviour of magma [1] will not be considered from a theoretical point of view; it is already incorporated indirectly into the experimental data. Furthermore, non-Newtonian behaviour of magma has a second order effect on the convection (Schowalter, 1978) and can therefore be neglected to first order.

The viscosity [2] of a typical magma could vary from 10 Pa·s to 10^{15} Pa·s, depending on a variety of factors (Williams and McBirney, 1979). In the next few sections I will examine briefly some of the most important factors that could influence the viscosity of magma.

3.2.1 Silicate Content

The viscosity of magma increases with increasing SiO_2 (silicate) content because silicate polymerises the melt to give long polymer chains which resist flow. A basalt, which has a Silicate content of about 50%, would have a viscosity of about 10^4 Pa·s at 1000°C while a rhyolite, with about 72% silicate would have a viscosity of 10^{10} Pa·s at the same temperature [3].

[1] The computer code being used can model non-Newtonian fluids but the viscosity data on magmas is not accurate enough to warrant the inclusion of this second order feature at present.

[2] Since the kinematic viscosity will not feature any further in this thesis, the dynamic Newtonian viscosity denoted by μ in equation (3.1), will from now on be referred to simply as viscosity.

[3] Both the quoted values are for a dry melt. The viscosities are remarkably similar when about 12% H_2O is added to both melts (Williams and McBirney, 1979). This is because

During the evolution of a magma chamber, the continual removal of high temperature components from the melt (either to the walls or as suspended load), as the melt cools, will lead to a more evolved melt, i.e. one with an higher silicate content. As a consequence of cooling the melt compositional changes thus occur. These changes can increase the viscosity of the evolving magma substantially and are a direct consequence of the change in composition (the increase in silicate content) rather than the decrease in temperature itself. Decreasing the temperature of the magma, while keeping the composition fixed, also increases the viscosity (Williams and McBirney, 1979), but this is a separate effect that will be discussed further in section 3.2.3.

3.2.2 Pressure

The effect of pressure on the viscosity of in magma is small compared to other effects like the variation of viscosity with silicate content. For example, an increase in pressure of about 5 atmospheres will lower the viscosity of an basaltic magma by only a few percent (Barnes, 1979).

It is generally agreed that the effect of increased pressure on basaltic and andesitic magmas is to decrease their viscosity. This decrease is attributed to a change in polymerisation (coordination of the silicate). One would however expect that the change in polymerisation would give rise to a step like change in viscosity but, instead, a continuous change in viscosity takes place as the pressure is varied. Why this occurs is not well understood (Williams and McBirney, 1979).

Granitic magmas that contain water also display the same viscosity pressure

water breaks the silicate bonds and de-polymerises the melt.

behaviour as above but, in this case, the behaviour is due to the increased solubility of water with increased pressure. Dissolved water tends to decrease the viscosity of granitic melts dramatically (Williams and McBirney, 1979).

In general, at the time of this writing, mechanisms for the effect of pressure on magma viscosity are not well understood. Progress in this field is retarded because accurate experimental data is hard to obtain and also very costly.

3.2.3 Temperature

The viscosity of all magmas increases monotonically with decreasing temperature. In regions where there are no crystals in the melt, i.e. above the liquidus, this increase is generally due to decreased molecular mobility. Below the liquidus, the change in viscosity is abetted by compositional changes that are an implicit consequence of the decrease in the temperature of the magma (See section 3.2.1). The formation of crystals in the melt causes the viscosity to increase more rapidly (with decreasing temperature) than it did above the liquidus. The viscosity of a melt that is below its liquidus is thus indirectly also function of time. As cooling proceeds, crystals grow in the melt and there are also more nucleation sites forming. Viscosity can thus increase even if the temperature is held constant. This last effect will be discussed in section 3.2.5.

3.2.4 Water Content

Water de-polymerises the melt thus causing a decrease in the viscosity. Since the silicate is responsible for polymerisation, the effect of adding water to

the melt is more pronounced in magmas which have higher silicate contents. Chemically, the H_2O disrupts the Si-Al framework (Williams and McBirney, 1979).

3.2.5 Time

If the temperature of a magma is held constant, below the liquidus temperature, the effective (bulk) viscosity of the magma and its crystal load increases because of the formation of crystals (Cox and Bell, 1978). This increase comes partly from the effect of increasing proportions of crystals which tend to raise the effective viscosity of the magma in which they are suspended, and partly from an increased ordering and polymerisation of the liquid. In viscosity measurements, the latter effect is typically offset by stirring (Williams and McBirney, 1979).

3.2.6 Viscosity data used in preliminary models

Viscosity data of magmas can be fitted by a general equation of the form

$$\mu = \mu_0 \exp\left\{V_2\left(\frac{1}{T} - \frac{1}{T_0}\right) + V_3\left(\frac{1}{T} - \frac{1}{T_0}\right)^2\right\} \tag{3.2}$$

where T_0 is the temperature at which the magma has a viscosity μ_0 and V_1 and V_2 are constants.

The viscosities that are used in the preliminary models of this thesis are all based on data taken by Murase and McBirney (1973). This data was obtained from experiments with magmas of various composition that were all approximately 35% crystallised for the duration of the experiment. Murase

and McBirney's viscosity data is shown by solid triangles in Figures 3.2, 3.3, 3.4 and 3.5. For the purposes of this thesis, the data has been fitted to equation (3.2) by linear regression using Microsoft Excel 1997.

The advantage of fitting equation (3.2) to the data, rather than fitting the more commonly used Arrhenius law, lies in the quadratic term

$$V_3\left(\frac{1}{T}-\frac{1}{T_0}\right)^2 \quad ,$$

which it contains. This term dominates in the behaviour of the viscosity at lower temperatures when $T << T_0$. At these temperatures it causes the viscosity to increase very rapidly as the magma cools and thus replicates the solidification process which typically occurs over a temperature range of less than 200°C of cooling. Equation (3.2) takes into account the effect of the suspended crystal load on the convection [4] and also, to a lesser extent, the finite yield strength that is expected in magmas. The observed behaviour of the viscosity of real magma with a crystal load is thus very close to that predicted by equation (3.2).

The values for the constants, V_2 and V_3 in equation (3.2), were obtained for each of the melts [5] shown in Table 3.1. The resulting curves from equation (3.2) are shown by solid lines in Figures 3.2, 3.3, 3.4 and 3.5. In each case, the viscosity is seen to be very large at lower temperatures where the magma is expected to behave as a solid, i.e. with a crystal load of more than 60%.

[4] When any magma crystallises to about 60% or higher it will behave essentially as a solid with viscosities of 10^{15} Pa·s or higher. See for example Williams and McBirney (1979).

[5] MHA ≡ Mount Hood Andesite, NRO ≡ Newberry Rhyolite Obsidian, CRB ≡ Columbia River Basal, SB ≡ Skaergaard Basalt

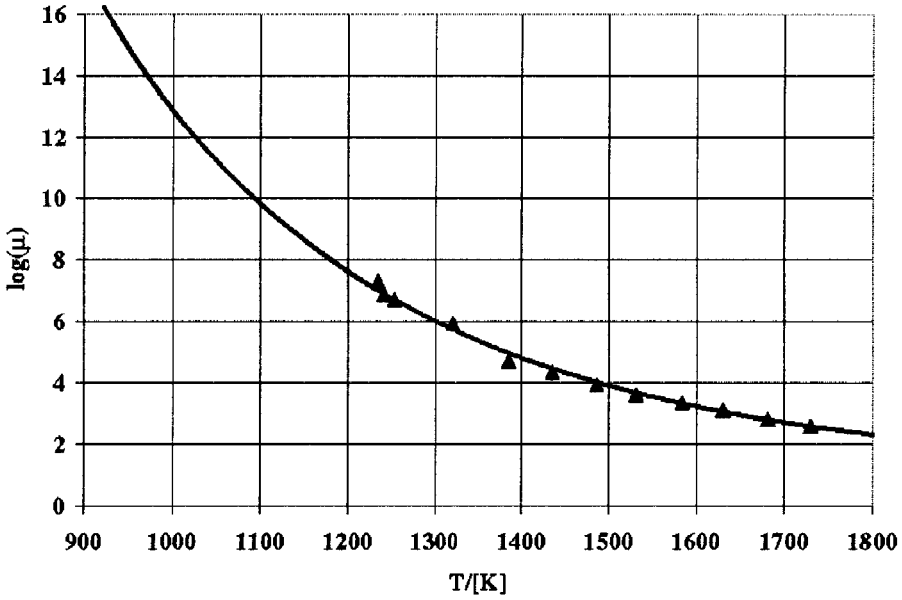

Figure 3.2: Log of the viscosity in Pa·s for the Mount Hood Andesite.

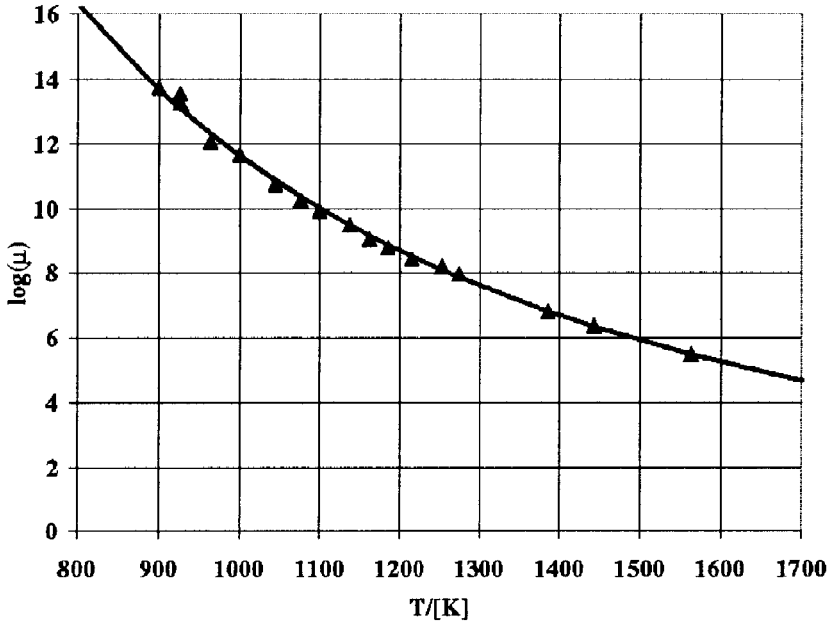

Figure 3.3: Log of the viscosity in Pa·s for the Rhyolite Obsidian.

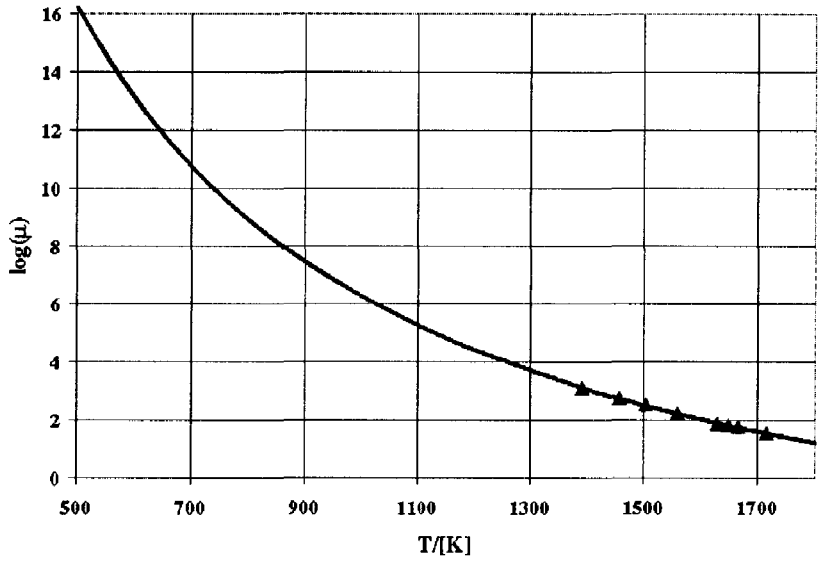

Figure 3.4: Log of the viscosity in Pa·s for the Columbia River Basalt.

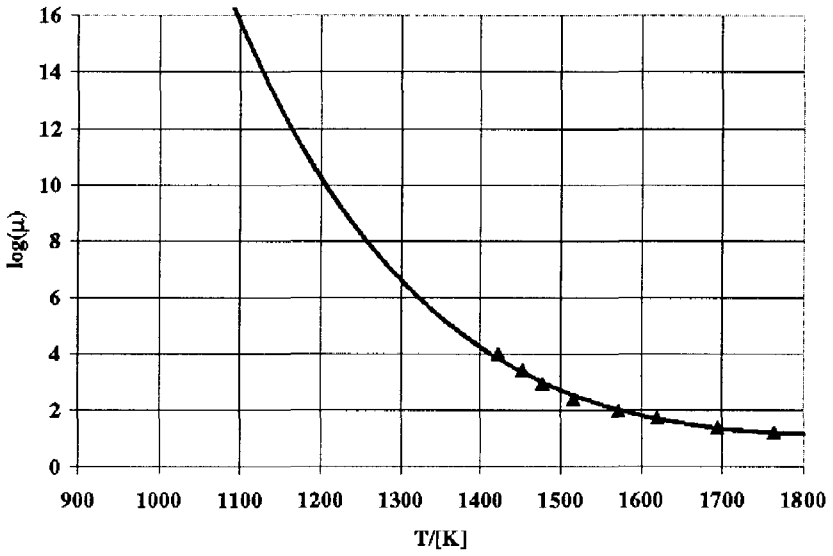

Figure 3.5: Log of the viscosity in Pa·s for the Skaergaard Basalt.

Table 3.1: Viscosity constants used in equation (3.2) based on various magma compositions from Murase and McBirney (1973). This equation includes the effect of the crystal load and thus models the solidification of the cooling chamber at low temperatures. See text for further details.

Magma	μ_0/[Pa · s]	T_0/[K]	V_2/[K]	V_3/[K^2]
MHA	7.37	1236	28881.34	64819537
NRO	8.61	1219	37003.14	6280087
CRB	1.96	1630	27052.99	-2229520
SB	5.02	1354	9638.731	257350403

3.3 Density

The density, ρ, of a magma varies mainly with temperature and chemical composition. Models which are based on chemical composition (See for example Bottinga and Weill (1970)) are generally only accurate above liquidus temperatures where the density increases linearly with decreasing temperature (Bottinga and Weill, 1970). The density of magma can however be modelled at all temperatures by a simple curve fit equation of the form

$$\rho = \rho_0 - \rho_0\beta(T - T_0) + \rho_0\gamma(T - T_0)^2 \tag{3.3}$$

In this equation, β is the coefficient of thermal expansion and ρ_0 is the density at the temperature T_0. The second (quadratic) term in (3.3) only contributes significantly when the magma is below its liquidus temperature, where $T << T_0$. It can be shown from thermodynamic considerations that the bulk density of the melt increases quadratically with temperature below

Table 3.2: Density constants used in equation (3.3) for the four different magma compositions. The quadratic dependence is included to model the crystal load that the magma may carry.

Magma	$\rho_0/[\mathrm{kg \cdot m^{-3}}]$	$T_0/[\mathrm{K}]$	$\beta/[10^{-5}\mathrm{K^{-1}}]$	$\gamma/[10^{-5}\mathrm{K^{-2}}]$
MHA	2500	1073	5.72	3.21
NRO	2220	1073	3.60	4.23
CRB	2820	1073	8.62	2.34
SB	2720	1073	7.35	3.91

the liquidus temperature of the magma (Brandeis and Jaupart, 1986). This is due to the fact that crystallisation takes place and this is a rate process, determined by the kinetics of nucleation and crystal growth.

3.3.1 Density data used in this thesis

The density of the magmas discussed in section 3.2.6 can be fitted to equation (3.3. This equation accounts for the effect of the crystal load by means of the quadratic term. The values obtained for the constants in equation (3.3) are listed in Table 3.2 for each of the magmas of section 3.2.6.

3.4 Thermal conductivity

Thermal conductivity is one of the most difficult physical properties to measure accurately. Even at room temperature typical measurements of ther-

mal conductivities have uncertainties of 10-20%. These uncertainties become larger at higher temperatures mainly because of the increase in the amount of thermal radiation present and the greater demands placed on the materials used to make the measurements (Snyder et al., 1994). It is not surprising therefore that very little empirical thermal data on magmas, typically at temperatures above 1000°C, is available. There are also no theoretical models that can predict the thermal conductivity of a magma of given composition. The principal reason for this is that magmas are generally very complex, eutectic systems. Even if the thermal behaviour of each component could be predicted, the overall thermal conductivity of the mixture does not depend simply upon the proportion of each component. For example, $MgAl_2O_4$ (spinel), which is made up of MgO and Al_2O_3, has a thermal conductivity considerably lower than either of its two constituents.

Magmas are notably poor conductors of heat. Up to the melting range, their thermal conductivity k, is approximately constant. Typically, in this region $k \approx 2$ J·m^{-1}s^{-1}K^{-1}. At higher temperatures, k varies according to the chemical composition of the melt (Williams and McBirney, 1979; Snyder et al., 1994). For mafic (silicate-poor) melts k generally decreases with increasing temperature up to about 1200°C. It then increases rapidly with temperature for temperatures above about 1200°C. In more siliceous melts k begins to increase at a much lower temperature. See Figure 3.6 for typical values of k. The variation in k can be explained in terms of the two mechanisms by which heat transfer takes place.

- **Photon conduction** - transfer of energy by radiation of photons
- **Phonon conduction** - transfer of energy by lattice vibrations

At high temperatures the translucency of the magma increases thus causing an increase in photon conduction, which is proportional to T^3. The translucency is determined by the amount of Fe^+ and Fe^{++} present in the melt. At high temperatures less of these two cations are present. There are thus less free electrons, and a corresponding decrease in skin depth, causing a higher translucency to photons (Chandrasekhar, 1957).

Melts that are siliceous thus have an high translucency at low temperatures and photon conduction dominates even while they are relatively cool. Their thermal conductivity thus increases with temperature, as T^3, even at very low temperatures as is shown for the NRO magma in Figure 3.6. In mafic melts the translucency is poor at low temperatures. Conduction is dominated by phonon conduction which tends to decrease the thermal conductivity linearly with increasing temperature. The overall conductivity of mafic melts thus first decreases linearly with temperature until it is dominated at higher temperatures by the photon conduction which is proportional to T^3. This behaviour is shown in Figure 3.6 for the mafic melts CRB, MHA and SB. These are the same magmas that were discussed in section 3.2.6. Other thermal conductivity data is also available (Snyder et al., 1994) and shows the same general trends as described above.

3.4.1 Thermal conductivity used for models in this thesis

The thermal conductivity of the magmas in this thesis are assumed constant. For most magmas this assumption is reasonably good over a limited temperature range (Williams and McBirney, 1979). Furthermore, thermal

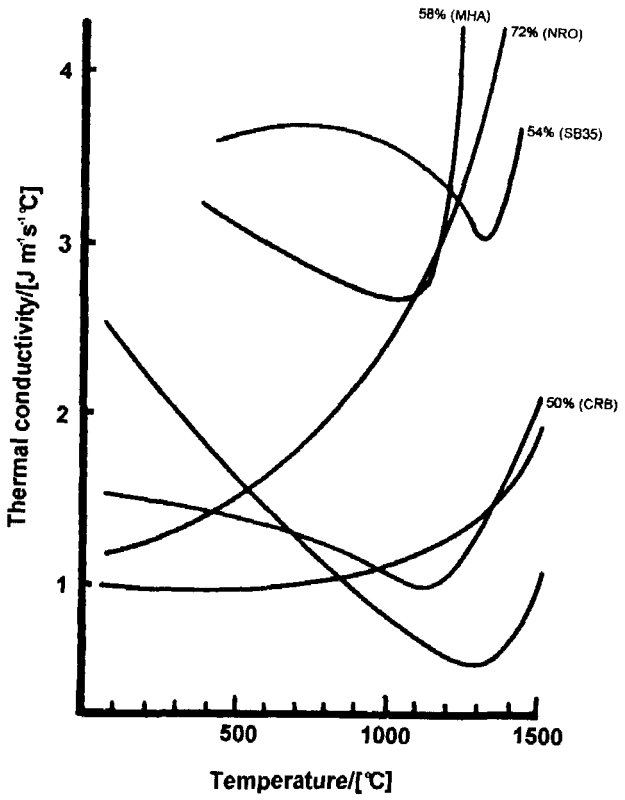

Figure 3.6: Typical thermal conductivity data illustrating the variations of thermal conductivity with temperature (See the text and also Appendix F). The Silicate content of 4 of the 6 curves is shown. The magmas in the labelled curves are the same as those discussed in chapter 6. From Williams and McBirney (1979).

conductivity data found in literature, although showing the same general trends, can differ by as much as one order of magnitude, compare for example data from (Snyder et al., 1994) and (Williams and McBirney, 1979). As a first approximation, it was therefore decided not to incorporate variable thermal conductivity into the models.

The above simplification, of taking k to be constant, is not a limitation of ANSYS 5.4. The variation of thermal conductivity can easily be accounted for in ANSYS by using the standard built in subroutines which allow one to program in any formula for k as a function of temperature (Spencer et al., 1997). The specific form of the function needed to fit thermal conductivity data has already been discussed in section 3.4 of this thesis. Although variable thermal conductivity has not been included in the present models, it will be included in future models by fitting data to the functional form discussed in section 3.4.

3.5 Specific Heat

For most solids it can be shown that $c_P \approx c_V$ i.e. the specific heats at constant pressure and at constant volume are about the same. This result is also approximately true (within 10 %) for solid igneous rocks (Williams and McBirney, 1979) and magmas. Magmas typically have approximately constant specific heats of about $1000\text{J} \cdot \text{kg}^{-1}\text{K}^{-1}$. Their specific heats at constant volume, c_V, and constant pressure, c_P, are also approximately equal.

The heat of fusion of a typical magma is

$$\Delta H_f \approx 4 \times 10^5 \mathrm{J} \cdot \mathrm{kg}^{-1} ,$$

and consequently, about the same amount of heat is required to cross the melting interval as is required to raise the temperature of the solid rock by about 400°C (Williams and McBirney, 1979). In order to model phase changes in magma, the enthalpy, rather than the specific heat, is thus used. This is because the specific heat becomes intractably large during a phase change. This complication is discussed further in section 4.2.3 in the context of the energy equation.

3.5.1 Specific heat used for models in this thesis

As for thermal conductivity, the specific heats of the magmas in this thesis are assumed constant, approximately equal to the value quoted for magmas in the previous section. [6] As already discussed, future models will make use of enthalpy to model the phase change in the magma. Even so, models that make use of constant specific are entirely valid for predicting flow patterns and many other important features of the convection in magma chambers as discussed in Rice et al. (1998).

[6] This is not because of deficiencies in the ANSYS code. Built in subroutines enables it to deal with phase changes in terms of enthalpy rather than specific heat (Spencer et al., 1997).

Chapter 4

Aspects of fluid mechanical models

4.1 Introduction

This section provides some background necessary for the understanding of the fluid mechanical aspects of models of magma chambers. It begins by introducing the equations, that govern the flow of Newtonian liquids, in their most general form. Simplifications that are made to these basic equations will be pointed out at a later stage.

4.2 Governing equations for magma

The equations that govern the flow of magma above its liquidus temperature are those for a Newtonian fluid. These equations are discussed in the next

few sections which refer to the symbols defined here:

$$
\begin{aligned}
e &= \text{internal energy / unit mass} \\
p &= \text{thermodynamic pressure} \\
T &= \text{temperature} \\
v_j &= \text{three components of velocity} \\
f_j &= \text{body force / unit mass} \\
k &= \text{thermal conductivity} \\
\lambda &= \text{second viscosity coefficient} \\
\mu &= \text{dynamic viscosity} \\
\rho &= \text{density} \\
h &= \text{enthalpy} \\
c &= \text{specific heat}
\end{aligned}
$$

4.2.1 Continuity equation

From the conservation of mass, it is possible to derive the continuity equation (Currie, 1993; Chorlton, 1967) in the form

$$\frac{\partial \rho}{\partial t} + \partial_k \left(\rho v_k\right) = 0 \quad \text{(sum over } k = 1, 2, 3) \tag{4.1}$$

An alternative form of the continuity equation is possible in terms of the substantial [1] derivative

$$\frac{D}{Dt} = \frac{\partial}{\partial t} + \boldsymbol{v} \cdot \nabla$$

[1] Sometimes also referred to as the material derivative or the particle derivative (Lamb, 1916).

which allows equation (4.1) to be written as

$$\frac{D\rho}{Dt} + \rho\nabla \cdot \boldsymbol{v} = 0\,,$$

where $\boldsymbol{v}$ is the velocity vector of the fluid with components $v_i = v_x, v_y, v_z$.

The physical interpretation of the substantial derivative is that it measures the time rate of change of a quantity while moving along with a fluid element (Lamb, 1916; Aris, 1962). The condition of incompressibility is therefore best expressed as

$$\frac{D\rho}{Dt} = 0 \quad \text{(incompressibility)}$$

and it now follows, from the continuity equation, in its second form, that the divergence of the velocity field is zero for incompressible flow. Thus for incompressible flow,

$$\partial_k v_k = \nabla \cdot \boldsymbol{v} = 0 \tag{4.2}$$

This last result will be used in the following sections.

4.2.2 Navier-Stokes equations

The Navier-Stokes equations are a set of three scalar equations, or one vector equation, for the velocity of a Newtonian fluid. They follow from the conservation of momentum and a full derivation can be found in Currie (1993). The resulting three Navier-Stokes equations are

$$\rho\frac{\partial v_j}{\partial t} + \rho v_k \partial_k v_j = -\partial_j p + \partial_j\left(\lambda\partial_k v_k\right) + \partial_i\left[\mu\left(\partial_j v_i + \partial_i v_j\right)\right] + \rho f_j \tag{4.3}$$

in component form. [2]

[2]These equations make use of the common abbreviation $\partial_i = \frac{\partial}{\partial x^i}$. See for example Currie (1993).

Equation (4.3) can be re-written in an alternative form by combining it with the continuity equation (4.1). This done, it emerges that

$$\frac{\partial}{\partial t}(\rho v_j) + \partial_k(\rho v_k v_j) = -\partial_j p + \partial_j(\lambda \partial_k v_j) + \partial_i[\mu(\partial_j v_i + \partial_i v_j)] + \rho f_j$$

or, if the incompressibility condition (4.2) is imposed,

$$\frac{\partial}{\partial t}(\rho v_j) + \partial_k(\rho v_k v_j) = \partial_i[\mu(\partial_j v_i + \partial_i v_j)] + \rho f_j - \partial_j p \qquad (4.4)$$

The above Navier-Stokes equations (4.4) are valid for incompressible flow. They have the form of the scalar transport equation that will be discussed in chapter 5.

4.2.3 Energy equation

The full derivation of the energy equation can be found in (Currie, 1993) where it is derived in the form

$$\rho\frac{\partial e}{\partial t} + \rho v_k \partial_k e = -p\partial_k v_k + \partial_j(k\partial_j T) + \lambda(\partial_k v_k)^2 + \mu(\partial_j v_i + \partial_i v_j)\partial_j v_i \quad (4.5)$$

Rewriting the left hand side of equation (4.5), using the continuity equation, and then imposing the incompressibility condition (4.2), equation (4.5) can be written as

$$\frac{\partial}{\partial t}(\rho e) + \partial_k(\rho v_k e) = \partial_j(k\partial_j T) + \Phi$$

where

$$\Phi = \mu(\partial_j v_i + \partial_i v_j)\partial_j v_i$$

is the dissipation function.

A more useful form of the energy equation is given in terms of enthalpy, h, where h is defined (See for example Lamb (1916)) by

$$h = e + \frac{p}{\rho}$$

With this substitution the energy equation can be written in terms of enthalpy as

$$\frac{\partial}{\partial t}(\rho h) + \partial_k(\rho h v_k) = \partial_k(k\partial_k T) + \Phi + \frac{Dp}{Dt}$$

This form of the energy equation will be used in chapter 5. It is worth noting that, in the case when c_P is constant, the enthalpy can be written in terms of temperature (Currie, 1993). In this case

$$h = cT.$$

This allows the energy equation to be written directly in terms of T but it is then valid only for cases when the specific heat is approximately constant. The more general approach is to deal with variable specific heat directly in term of enthalpy. This allows for modelling of phase changes where the specific heat of the magma usually varies substantially. Also see Bird, Stewart and Lightfoot (1963).

4.2.4 Equations of state

In addition to the above five equations, two additional mechanical equations of state are required to complete the set of seven governing equations (Currie, 1993). These are, the mechanical equation of state

$$p = p(\rho, T) \tag{4.6}$$

and, the heat equation of state

$$e = e(\rho, T) \tag{4.7}$$

For further details concerning the governing equations, see for example Currie (1993), Batchelor (1967) or Aris (1962). In the past, further simplifications (other than those listed above) have been made to the governing equations in order to obtain initial results with minimal computational power. These simplifications, and their applicability to magma chambers, have been discussed in, for example, Botha et al. (1997) or Harrison et al. (1997).

The assumption of incompressibility is not essential to our formulation and is made here only to show, more simply, how the governing equations can all be cast in the form of the generic scalar transport equation discussed in section 5.3.1 (Botha et al., 1996b; Botha et al., 1996a). ANSYS 5.4 is fully capable of solving the most general governing equations. Even though the preliminary results in this thesis make use of further simplifications (see chapter 6), the full set of governing equations can be solved by the computer code, even in the case of compressible flow. This will be discussed further in chapter 5.

The simplifications we make are not as restrictive as those usually found in literature (Sparks and Huppert, 1984; Turner, 1980; Hansen, 1987): we have, for example, retained the complete set of streaming terms in the momentum equation, see section 5.3.1. Further advantages of our approach are discussed in Harrison (1998).

4.3 Convection inside magma chambers

All magma chambers of appreciable size, but especially those with lower silicate content, will typically undergo vigorous convection. This may be ascertained from the Rayleigh number of the magma chamber, Ra. The

Rayleigh number, for convection between two flat horizontal plates of infinite extent, is defined in Appendix D. A derivation of this particular Rayleigh number can be found on page 330 of Currie (1993). This derivation employs standard perturbation techniques to linearise the governing equations. The perturbation quantities are then represented by Fourier integrals and from the resulting eigenvalue problem it is deduced that there exists a critical value of the Rayleigh number Ra_c, beyond which the perturbations grow in time to produce convective motion. Below the critical Rayleigh number all possible disturbances decay and thus no convection takes place.

It is found from the above analysis that $Ra_c = 1707.8$ for non-slip boundary conditions and $Ra_c = 1100.7$ when one of the boundaries is free. Experimental results are in accordance with both of these predicted values and the theory can be said to explain the onset of convection successfully in the case of flat horizontal plates. See pages 217-219 of Tritton (1977).

Even though the geometry of a typical magma chamber does not conform to the exact geometry used in defining the above Rayleigh number, the above definition can still be used to characterise the vigour of the convection within a magma chamber (Williams and McBirney, 1979). The critical values, that are listed above, will of course not be applicable to a magma chamber. Even so, dimensional scaling, and accurate numerical solutions to the governing equations, can be used to infer approximate values of Ra applicable to magma chambers.

The Rayleigh number is generally a monotonic increasing function of the ratio of heat which is convected to heat which is conducted, i.e. it is a function of

the Nusselt number, Nu. We can thus write, quite generally,

$$Nu \propto Ra^n = Ra^n \left(\frac{\text{heat convected}}{\text{heat conducted}} \right) \tag{4.8}$$

It is found experimentally that, in the above equation, and for a large variety of geometries,

$$\begin{aligned} n &= \frac{1}{4} \quad , \text{ for laminar flow, and} \\ n &= \frac{1}{3} \quad , \text{ for turbulent flow.} \end{aligned}$$

Thus, if heat transfer is mainly by conduction, Ra will be lower than in the case where heat transfer is mainly by convection. As convective heat transfer within the magma increases, the Rayleigh number also increases. Therefore, above the critical value, Ra_c, heat transfer is no longer purely conductive, but also takes place as a result of convection. A practical approximation [3] for this critical value is usually taken to be equal to the case of flat horizontal plates.

From the definition of the Rayleigh number as

$$Ra = \frac{g\beta\rho^2 d^3 \Theta}{\mu k},$$

it is seen that Ra will decrease as the magma chamber evolves. This is because

- as the magma cools and the country rock heats up, the temperature difference Θ decreases, thus causing Ra to decrease.
- as the magma cools it becomes more viscous, thus μ increases causing Ra to decrease.

[3] Ra_c may vary if there is a concentration gradient in the fluid. See Rice (1981) for references.

- as solidification proceeds along the (cooler) sides of the magma chamber, the convecting part of the chamber shrinks and thus the factor d^3 in the Rayleigh number decreases. This causes Ra to decrease all the way to zero, when no more convection occurs since the chamber has solidified.

The highest power occurring in (4.54) is 3, and only one variable, d, occurs with this power. This means that the depth of the fluid is the most influential variable in determining the value of the Rayleigh number. For a typical magma chamber Ra can range from about 10^{14} initially, to below 1700, as the magma freezes.

Convective velocities of magma can be estimated from the ratio of the streaming terms to the viscous terms in the Navier-Stokes equations for fluid flow (Tritton, 1977; Rice and Eales, 1995). For large Grashof numbers, Gr,

$$\frac{\rho|\boldsymbol{v}\cdot\nabla\boldsymbol{v}|}{\mu\nabla^2\boldsymbol{v}} \approx \frac{vd\rho}{\mu} = Gr^{1/2} \tag{4.9}$$

where v is the magnitude of the velocity. Gr is related to the Rayleigh number by the relation

$$Gr = \frac{Ra}{Pr} \tag{4.10}$$

where $Pr = \mu c/k$ is the Prandtl number and c is the specific heat.

Solving for v in equation (4.9) and using equation (4.10) with the definitions of Ra and Pr given above, produces

$$v = \sqrt{g\beta d\Theta} \tag{4.11}$$

Inserting typical values for a basaltic melt into the right hand side of equation (4.11), it is found that

$$v = \sqrt{(9.81\mathrm{m}\cdot\mathrm{s}^{-2})(5.09\times10^{-5}\,^{\circ}\mathrm{C}^{-1})(1000\mathrm{m})(20^{\circ}\mathrm{C})} \;=\; 3.16\mathrm{m}\cdot\mathrm{s}^{-1} \tag{4.12}$$

This gives an estimate for the velocity of a convecting magma in a chamber which is about 1000 m deep. For an estimate of the convective velocity at which convection will commence, v_c, use can be made of the following relation from Tritton (1977). Inserting the above values,

$$v_c = \frac{\mu}{\rho d}\left(\frac{Ra_c}{Pr}\right) = \frac{28}{2800 \times 1000}\left(\frac{1700}{10^4}\right) = 1.7 \times 10^{-6}\mathrm{m} \cdot \mathrm{s}^{-1} \qquad (4.13)$$

In the above situation, convection will thus play an important role in the cooling history. According to the above calculation the critical velocity is about six orders of magnitude less than a typical convective velocity.

4.4 The equation of heat conduction

This section develops the analytic solution to the problem of conductive cooling in a finite cylinder. The basic method employed here is from Carslaw and Jaeger (1959), although substantial changes in notation have been implemented to attain a consistency with the notation employed in this thesis. Furthermore the sections below are an elaboration on one very brief section of less than a page in Carslaw and Jaeger (1959).

The analytic solution to the problem of heat conduction in a finite cylinder (Carslaw and Jaeger, 1959) will be now be used to estimate the cooling time of a magma chamber of similar geometry. There is no known analytic solution to the equations that govern the convection that occurs inside the chamber and at best, we are able to obtain an estimate of the cooling time by enhancing the thermal conductivity through use of the Nusselt number, Nu, in the known analytic solution for conduction. By this method the chamber first treated analytically as a solid which cools by conduction only. By using

an effective conductivity for the chamber, the product of the Nusselt number and the actual conductivity, k, an estimate of the convective cooling time of the chamber is obtained without solving the details of the actual convection that occurs inside the chamber. This estimate can then be compared to the numerical solution of the convection inside the chamber as computed by the ANSYS 5.4 finite element package. The outcome of the calculations confirm that, in the simple case of finite cylindrical magma chambers, the ANSYS [4] code produces results that are consistent with the analytic solution outlined above.

4.4.1 Simplification

Let $T'(x, y, z, t)$ be the temperature of a system with an initial temperature distribution $T_i(x, y, z)$ at time $t = 0$. Let $T_b(x, y, z)$ be a solution to the steady state equation of heat conduction for the system (it does not change with time) then the function

$$T = T' - T_b$$

will satisfy the equation of conduction

$$\frac{\partial T}{\partial t} = \kappa \nabla^2 T \tag{4.14}$$

subject to the boundary conditions:

$$T(x, y, z, 0) = T_i(x, y, z) - T_b(x, y, z) \tag{4.15}$$

at time $t = 0$, and on the surface,

$$T(x, y, z) = 0 \tag{4.16}$$

[4]General information about ANSYS 5.4 can be obtained from the ANSYS web-site: http://www.ansys.com.

Here $\kappa = k/(\rho c)$ (SI units: m^2/s) is the thermal diffusivity [5]. Now, in the case when the surface boundary conditions do not depend on time, the general problem of heat conduction reduces to two problems: that of finding

- the steady state solution $T_b(x, y, z)$ and
- the solution T, subject to the simplified (zero) boundary condition given in (4.16) above.

We will make use of this result in subsequent sections for the case where the boundary temperature is constant over the entire surface. In this case the solution to the steady state problem is just the constant boundary temperature. In more complicated cases, where the temperature on the boundary takes into account the geothermal gradient surrounding the chamber, the steady state solution is more complicated. For simplicity, a constant boundary temperature will be used in what follows to illustrate how the above technique can be allied.

4.4.2 Finite cylinders

Consider a cylinder of length $2l$ and radius a positioned with its centre at the origin of a Cartesian coordinate system with the z-axis in the direction of the length of the cylinder. Let the initial internal temperature distribution of the cylinder be $T_i(x, y, z)$ and let the surface temperature be zero in view of the discussion in section 4.4.1. In cylindrical coordinates it is possible to express the initial and boundary conditions given respectively by equations

[5] As before: k = thermal conductivity, rho = density, c = specific heat

(4.15) and (4.16) above as

$$\begin{aligned} T(r,\theta,z,0) &= T_i(r,\theta,z) \\ T(a,\theta,z) &= T(r,\theta,\pm l) = 0 \end{aligned}$$

where $T(r,\theta,z,t)$ satisfies the equation of conduction, which in cylindrical coordinates, takes the form

$$\frac{1}{\kappa}\frac{\partial T}{\partial t} = \frac{\partial^2 T}{\partial r^2} + \frac{1}{r}\frac{\partial T}{\partial r} + \frac{1}{r^2}\frac{\partial^2 T}{\partial \theta^2} + \frac{\partial^2 T}{\partial z^2} \tag{4.17}$$

This equation can be solved by separation of variables (Kreith and Bohn, 1993) by assuming a solution of the form

$$T(r,\theta,z,t) = A(t)B(r)C(\theta)D(z) \tag{4.18}$$

Substituting (4.18) into (4.17) and dividing by $A(t)B(r)C(\theta)D(z)$ produces

$$\frac{1}{\kappa A}\frac{\partial A}{\partial t} = \frac{1}{B}\frac{\partial^2 B}{\partial r^2} + \frac{1}{rB}\frac{\partial B}{\partial r} + \frac{1}{r^2 C}\frac{\partial^2 C}{\partial \theta^2} + \frac{1}{D}\frac{\partial^2 D}{\partial z^2} \tag{4.19}$$

Since the left hand side of (4.19) is dependent only on time while the right hand side does not depend on time, each side of (4.19) must be equal to constant. Furthermore since κ is positive and the derivative on the left hand side is assumed negative, the separation constant is written as $-\nu^2$. This produces two equations:

$$\frac{1}{\kappa A}\frac{\partial A}{\partial t} = -\nu^2 \tag{4.20}$$

$$\frac{1}{B}\frac{\partial^2 B}{\partial r^2} + \frac{1}{rB}\frac{\partial B}{\partial r} + \frac{1}{r^2 C}\frac{\partial^2 C}{\partial \theta^2} + \frac{1}{D}\frac{\partial^2 D}{\partial z^2} = -\nu^2 \tag{4.21}$$

Reorganising (4.21) yields

$$\frac{1}{B}\frac{\partial^2 B}{\partial r^2} + \frac{1}{rB}\frac{\partial B}{\partial r} + \frac{1}{r^2 C}\frac{\partial^2 C}{\partial \theta^2} = -\frac{1}{D}\frac{\partial^2 D}{\partial z^2} - \nu^2 \tag{4.22}$$

and as before, both sides of this equation are equal to a negative constant, say $-\mu^2$. Thus from (4.22),

$$\frac{1}{B}\frac{\partial^2 B}{\partial r^2} + \frac{1}{rB}\frac{\partial B}{\partial r} + \frac{1}{r^2 C}\frac{\partial^2 C}{\partial \theta^2} = -\mu^2 \tag{4.23}$$

$$-\frac{1}{D}\frac{\partial^2 D}{\partial z^2} - \nu^2 = -\mu^2 \tag{4.24}$$

where (4.23) can still be further separated by multiplying through by r^2 and rearranging to get

$$\frac{r^2}{B}\frac{d^2 B}{dr^2} + \frac{r}{B}\frac{\partial B}{\partial r} = -\frac{1}{C}\frac{d^2 C}{d\theta^2} - \mu^2 r^2 \tag{4.25}$$

Equation (4.25) can be separated as before to give

$$\frac{r^2}{B}\frac{d^2 B}{dr^2} + \frac{r}{B}\frac{dB}{dr} + r^2\mu^2 = -\lambda^2 \tag{4.26}$$

$$-\frac{1}{C}\frac{d^2 C}{d\theta^2} = -\lambda^2 \tag{4.27}$$

Thus a function of the type (4.18) is a solution to equation (4.17) if and only if its factors A, B, C and D are solutions of the following 4 independent ordinary differential equations.

$$\frac{1}{A}\frac{dA}{dt} = -\kappa\nu^2 \tag{4.28}$$

$$r^2\frac{d^2 B}{dr^2} + r\frac{dB}{dr} + \left(r^2\mu^2 + \lambda^2\right)B = 0 \tag{4.29}$$

$$\frac{d^2 C}{d\theta^2} - \lambda^2 C = 0 \tag{4.30}$$

$$\frac{d^2 D}{dz^2} + \left(\nu^2 - \mu^2\right)D = 0 \tag{4.31}$$

The solution to equation (4.28) is

$$A(t) = e^{-\kappa\nu^2 t} \tag{4.32}$$

Equations (4.30) and (4.31) each have the form of the equation for simple harmonic motion. The solution to (4.30) is therefore

$$C(\theta) = \sin(\lambda\theta) \tag{4.33}$$

where, for convenience, the phase angle has been chosen to be zero and the amplitude set equal to unity. Similarly, for (4.31), a solution is given by

$$D(z) = \sin\left[z\sqrt{\nu^2 - \mu^2} + z_0\right] \tag{4.34}$$

Although the amplitude of $D(z)$ may be freely set to unity, it is necessary to impose the boundary conditions

$$D(-l) = D(+l) = 0$$

to get the appropriate phase (Carslaw and Jaeger, 1959).

Substituting the boundary condition into (4.34), we obtain the relation

$$2l\sqrt{\nu^2 - \mu^2} = m\pi \quad m = 1, 2, 3, ... \tag{4.35}$$

Because of the circular symmetry in the theta equation, an integral multiple of the period of C, must be equal to 2π i.e. $\lambda = 1, 2, 3, ...$ in equation (4.33).

Equation (4.29) is Bessel's equation. It has particular solutions given by Bessel functions of the first kind. With the requirements that $B(\mu a) = 0$ and that $B(\mu r)$ be finite at the origin, the particular solutions to equation (4.29) are of the form

$$J_n(\mu r) \quad n = 0, 1, 2, ...$$

where J_n denotes a Bessel function of the first kind.

Since r is restricted to be positive or zero, the constants μ are the positive zeros of the equation

$$J_n(\mu a) = 0 \tag{4.36}$$

This restriction comes from the boundary condition $B(\mu a) = 0$.

The separable solutions are thus of the form

$$\begin{aligned} T_{\mu nm}(r,\theta,z,t) &= e^{-\kappa\left(\mu^2+\frac{m^2\pi^2}{4l^2}\right)t} J_n(\mu r)\sin(n\theta)\sin\left[\frac{m\pi}{2l}(z+l)\right] \\ &+ e^{\kappa\left(\mu^2+\frac{m^2\pi^2}{4l^2}\right)t} J_n(\mu r)\cos(n\theta)\sin\left[\frac{m\pi}{2l}(z+l)\right] \end{aligned}$$

where $m = 1, 2, 3, \ldots$ and the μ are the positive roots of equation (4.36).

The general solution is then

$$T(r,\theta,z,t) = \sum_{\mu}\sum_{m=1}^{\infty}\sum_{n=0}^{\infty} T_{\mu nm}(r,\theta,z,t) \tag{4.37}$$

To apply the initial condition that $T = T_i(r,\theta,z)$ at time $t = 0$, $T_i(r,\theta,z)$ must be appropriately expanded. The first expansion of $T_i(r,\theta,z)$ is as a Fourier series

$$T_i(r,\theta,z) = \frac{F_0(r,z)}{2} + \sum_{n=1}^{\infty}\left(F_n(r,z)\cos(n\theta) + G_n(r,\theta)\sin(n\theta)\right) \tag{4.38}$$

where

$$F_n(r,z) = \frac{1}{\pi}\int_{-\pi}^{+\pi} f(r,\theta,z)\cos(n\theta)d\theta \tag{4.39}$$

$$G_n(r,z) = \frac{1}{\pi}\int_{-\pi}^{+\pi} f(r,\theta,z)\sin(n\theta)d\theta \tag{4.40}$$

The second expansion of $F_n(r,\theta)$ and $G_n(r,\theta)$ is in terms of a series of Bessel functions given by the positive roots of $J_n(\mu a) = 0$ i.e.

$$F_n(r,z) = \frac{2}{a^2[J_n'(\mu a)]^2}\sum_{\mu} c_{\mu n}(z)J_n(\mu r) \tag{4.41}$$

$$G_n(r,z) = \frac{2}{a^2[J_n'(\mu a)]^2}\sum_{\mu} d_{\mu n}(z)J_n(\mu r) \tag{4.42}$$

where $c_{\mu n}(z)$ and $d_{\mu n}(z)$ are even functions of z and can therefore be expanded as a sine series i.e.

$$c_{\mu n}(z) = \sum_{m=1}^{\infty} A_{\mu nm}\sin\frac{m\pi}{2l}(z+l) \tag{4.43}$$

$$d_{\mu n}(z) = \sum_{m=1}^{\infty} B_{\mu nm}\sin\frac{m\pi}{2l}(z+l) \tag{4.44}$$

where

$$A_{\mu nm} = \frac{1}{l}\int_{-l}^{+l} c_{\mu n}(z)\sin\frac{m\pi}{2l}(z+l) \tag{4.45}$$

and $B_{\mu mn}$ is given by an analogous expression.

Now, substituting the expansions of $c_{\mu n}$ and $d_{\mu n}$ into these expressions shows that

$$A_{\mu mn} = \frac{2}{\pi a^2[J_n'(\mu a)]^2}\int_{-l}^{+l}\int_0^a\int_{-\pi}^{+\pi} r\cos(n\theta)f(r,\theta,z)J_n(\mu r)\sin\left[\frac{m\pi}{2l}(z+l)\right]d\theta dr dz$$

Again, $B_{\mu mn}$ is treated similarly which thus expands the boundary temperature distribution so that it has exactly the same form as the general solution to the conduction equation at time $t = 0$. Thus the general solution is given by

$$T=\sum_\mu\sum_{m=1}^{\infty}\sum_{n=0}^{\infty} e^{-\kappa\left(\mu^2+\frac{m^2\pi^2}{4l^2}\right)t} J_n(\mu r)\sin\left[\tfrac{m\pi}{2l}(z+l)\right](A_{\mu mn}\cos(n\theta)+B_{\mu mn}\sin(n\theta))$$

where

$$A_{\mu mn} = \frac{2}{\pi a^2[J_n'(\mu a)]^2}\int_{-l}^{+l}\int_0^a\int_{-\pi}^{+\pi} r\cos(n\theta)f(r,\theta,z)J_n(\mu r)\sin\left[\frac{m\pi}{2l}(z+l)\right]d\theta dr dz$$

and $B_{\mu mn}$ is given by a similar expression (Carslaw and Jaeger, 1959).

Notice that because the first term in the Fourier expansion of $f(r,\theta,z)$ is halved, the expression for the A and B must be halved when n is equal to zero.

4.5 Convective cooling of a finite cylinder

By weighting the thermal conductivity with the Nusselt number the above results can be used to obtain estimates of the convective cooling time of a finite cylinder as shown below. The first step is to modify the thermal conductivity using an appropriate correlation function for the heat transfer in a finite cylinder.

For purely conductive heat loss in one dimension the time taken for the main body of fluid to cool to $1/e$ of its original value is given by

$$\tau = \frac{d^2}{\kappa} \tag{4.46}$$

where κ is the thermal diffusivity of the fluid (Kreith and Bohn, 1993). To estimate the time constant of convective heat loss it is necessary to work with an effective thermal diffusivity $\tilde{\kappa}$. Comparison of Newton's law of cooling (See equation (4.54) of section 4.5.3), written in the form

$$q = h\Delta T \;=\; \frac{kNu}{d}\Delta T\,, \tag{4.47}$$

and the equation of heat conduction,

$$q = k\frac{dT}{dx} \;\approx\; \frac{k}{d}\Delta T \tag{4.48}$$

shows that the effective thermal conductivity is given by $\tilde{k} = kNu$, where the Nusselt number, $Nu = hd/k$, and h is called the heat transfer or film coefficient. From this we see that the effective thermal diffusivity is

$$\tilde{\kappa} = \frac{\tilde{k}}{\rho c} \;=\; Nu\kappa \tag{4.49}$$

where ρ is the density of the fluid and c, specific heat. Using this result, it is possible to obtain an estimate of the cooling time of a system in which heat

transfer is by conduction and convection. By analogy to equation (4.46) the e-folding time will be of the order $\tilde{\tau}$, where

$$\tilde{\tau} = \frac{d^2}{\tilde{\kappa}} = \frac{d^2}{Nu\ \kappa} \tag{4.50}$$

This result will be used in section 4.5.1.

A correlation function for natural-convective heat transfer to the walls of a cylinder may be derived by plotting the average Nusselt number on the surface of the cylinder, $\bar{Nu}$, as a function of the Rayleigh number defined for the cylinder. Direct experimental work with large cylindrical magma chambers is not necessary since it is possible to make use of dynamic similitude to extend existing experimental work on smaller models to magma chambers. Alternatively, finite element analysis can be used to derive the appropriate correlation function. However, since the present purpose is only to find the approximate initial value of $\bar{Nu}$, a correlation function for cylinders will not be derived here. Instead, a correlation function for melting in a vertical cylinder (Farid et al., 1989) will be used to show that the ANSYS code produces results that are consistent with experimentally derived correlation functions in the case of cylindrical models.

The experimental correlation function is (Farid et al., 1989)

$$\bar{Nu} = 0.28 Ra^{1/4} \quad , \quad 2 \times 10^3 < Ra < 1 \times 10^7 \tag{4.51}$$

From this it is evident that a cylindrical magma chamber with a Rayleigh number of about 1.6×10^6, will have a corresponding Nusselt number, $Nu = 9.95$. Heat flux data from cylindrical models computed with ANSYS and having the same initial Rayleigh number, gives a Nusselt number between 9.5 and 10.5. The two results are thus consistent to within a few percent; another important bench-mark calculation. For higher Rayleigh numbers,

where different correlation functions apply (See for example equation (4.57) of section 4.5.3.), the initial Nusselt numbers that can be computed from the ANSYS heat flux data agree to a similar extent with theoretical values found from correlation functions.

4.5.1 Application to cooling times

By comparing the initial conductive heat transfer to the walls of the cylinder to the initial convective heat transfer, a Nusselt number for the cylinder can be calculated. This was done for the rhyolitic cylindrical in magma chamber of chapter 6 and Nu was found to be about 18. The rhyolitic cylinder thus has an effective thermal diffusivity, $\tilde{\kappa} = Nu\kappa \approx 36$.

By evaluating the solution to the finite cylinder problem (See the last two equations of section 4.4.2.) at the centre of the cylinder (where $r = 0$ and thus $J_0(0) = 1$) it can be seen that the temperature distribution at the centre is given by

$$T = \sum_{\mu} \sum_{m=1}^{\infty} e^{-\kappa\left(\mu^2 + \frac{m^2\pi^2}{4l^2}\right)t} \sin\left[\frac{m\pi}{2}\right] A_{\mu m n} \tag{4.52}$$

As the terms in this series rapidly tend to zero with increasing values of m and μ, the first few terms give an approximate expression for the temperature in the centre of the cylinder as it cools by pure conduction. Alternatively, if κ is replaced by the effective conductivity, $\tilde{\kappa}$, we obtain the cooling curve for the centre of the cylinder with convection. This cooling curve is shown by the dotted curve (marked **Bessel**) in Figure 4.1 for the rhyolitic cylinder discussed in chapter 6, section 6.3.

A comparison of the analytic approximation, as derived above in equation (4.52), and the numerical solution for convection in a finite circular cylinder,

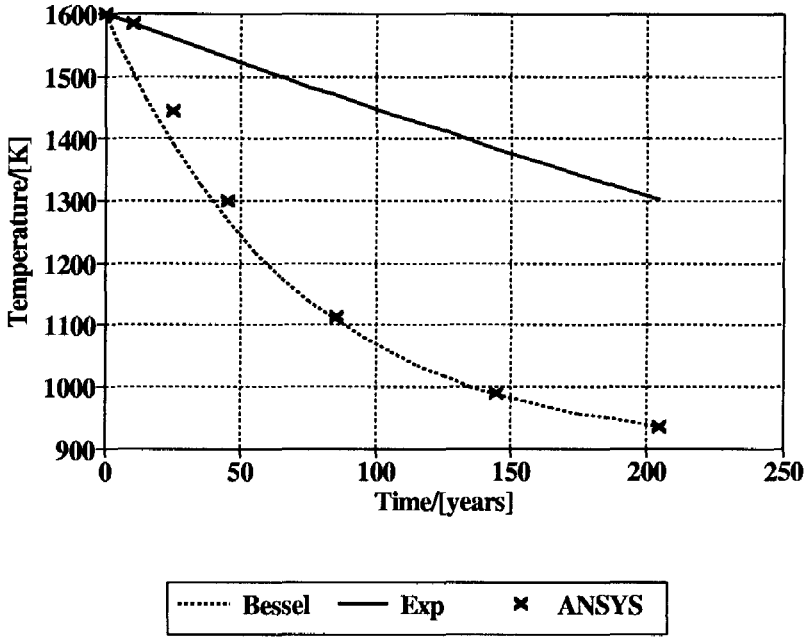

Figure 4.1: Comparison of the analytic heat conduction solution for a finite circular cylinder (marked **Bessel**) to the finite element solution (marked **ANSYS**) and an exponential approximation to this problem by the one dimensional cooling solution (marked **Exp**). In the Bessel function solution and in the one dimensional solution an effective thermal diffusivity, $\tilde{\kappa} = Nu\kappa$, is used to replicate the actual convection that can be modelled directly by ANSYS 5.4. A very good agreement is seen between the analytic solution and the ANSYS code.

obtained from ANSYS 5.4, is shown in Figure 4.1. This figure also includes a plot of the familiar exponential solution,

$$T = 1600 \exp\left(\frac{Nu\ \kappa\ t}{a^2}\right) , \tag{4.53}$$

to the problem of heat conduction in one dimension (i.e. for a thin conducting strip with an initial temperature equal to the internal initial temperature of the cylinder at its centre ($1600°C$) and a length equal to the radius of the

cylinder.) with the effective conductivity applicable to the cylinder. This last solution is frequently used in literature to estimate the cooling times of magma chambers of all shapes and sizes.

It can be seen from Figure 4.1, that the analytic solution for conduction, using the modified thermal diffusivity to mimic convection, agrees almost exactly with the finite element solution obtained from ANSYS 5.4 for the actual convection. It is also clear that the one dimensional approximation (**Exp**) is not accurate when applied to the cylindrical geometry, even when the effective conductivity has been used, as in this case.

4.5.2 Undercooling in Magma

The phenomenon of undercooling is very important to crystallisation in magma chambers. When magma freezes, latent heat of crystallisation is released. This heat is readily re-absorbed into the magma and will thus tend to inhibit further cooling of the melt unless it is released into the surrounding country rock. Crystallisation occurs where the magma has cooled to below its liquidus temperature and the release of latent heat provides the activation energy necessary to secure further freezing. See the graph in Figure 4.2 which shows the critical radius compared to temperature and nucleation free energy, ΔG. Without it, freezing would stop since it is required that the nucleation energy (total free energy) $\Delta G < 0$ for the formation of a crystal (Vlack, 1964). The nucleation energy, ΔG, is thus a potential barrier which the molecules must overcome in order to combine into crystals. The release of latent heat provides the molecules with the necessary kinetic energy to overcome the potential barrier in order to form crystals and does not, as

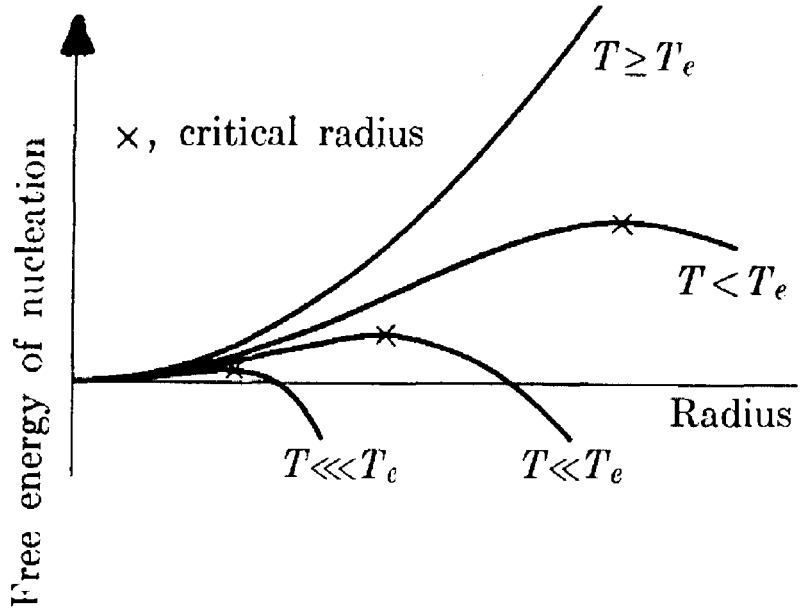

Figure 4.2: Critical nucleation radius compared to temperature and melt free energy ΔG. The amount of undercooling is the difference between the equilibrium transformation temperature (e.g. melting point) T_e and the actual temperature T. Additional undercooling decreases the critical radius and therefore increases the probability of nucleation. From Vlack (1964).

sometimes thought, exclude the possibility of further crystallisation.

Although the release of latent heat will tend to stabilise the temperature of the magma at its liquidus temperature, the country rock surrounding the chamber could easily be capable of removing latent heat fast enough to ensure a temperature drop well below the liquidus. This phenomenon is known as undercooling.

The extent of undercooling that takes place in a magma chamber has been discussed in Rice (1995). Typically a magma could be expected to experience undercooling of about 20 °C below its liquidus temperature and certainly much more at the walls immediately after emplacement.

4.5.3 Boundary layer thickness

The wall boundary layer is defined as the region extending from the wall, where convective velocities are zero, to where the velocities assume mainstream values. From the definition of viscosity (Section 3.2) it can be seen that the shear forces within the magma will be largest within the boundary layer. The boundary layer thickness is important, since it is the region where the most shearing takes place. Shearing in the magma could be responsible for the enrichment in certain minerals like PGEs (Rice and von Gruenewaldt, 1994). This section demonstrates a common method of estimating the boundary layer thickness of a typical magma chamber.

Conductive heat flow across a surface is governed by Newton's law of cooling,

$$q = h\Delta T \tag{4.54}$$

where q is the heat transferred per unit time per unit area, h is the film coef-

ficient, and ΔT is the temperature difference [6] between the surface temperature of the fluid and the bulk temperature of the fluid. The film coefficient h is given by

$$h = kNu/d \tag{4.55}$$

where k is the thermal conductivity, d is the characteristic dimension normal to the boundary of the fluid and spanning the temperature difference ΔT, and Nu is the Nusselt number. Nu can be related to the Rayleigh number by an equation of the form

$$Nu = ARa^n \tag{4.56}$$

where the values of A and n are experimentally determined constants for a small range about the Rayleigh number of interest. For turbulent flow between flat plates $A = 0.13$ and $n = 1/3$ (Tritton, 1977). Thus equation (4.56), for this situation is

$$Nu = 0.13Ra^{1/3} \quad , \quad 10^7 < Ra \tag{4.57}$$

In this range, the Nusselt number can be expressed in terms of the boundary layer thickness as (Tritton, 1977)

$$Nu = d/\delta \tag{4.58}$$

and the boundary layer thickness δ can be approximated in terms of the Rayleigh number. From equations (4.58), (4.57), (4.55), and (4.54) it is evident that

$$\delta \approx 7.7dRa^{-1/3} \tag{4.59}$$

[6] The definition of ΔT differs if heat transfer takes place during flow past an immersed body. In this case $\Delta T = T_s - T_\infty$, where T_∞ is the temperature of the fluid which is not disturbed by the immersed body and T_s is the temperature of the fluid at the surface of the body.

Thus for a magma chamber that is 1km thick convecting at a Rayleigh number of $Ra \approx 10^{12}$, a boundary layer thickness of $\delta \approx 1m$ is derived from equation (4.59). It is worth noting that this value is consistent with the extent of undercooling that can be expected in a typical magma chamber.

The observed boundary layer thicknesses in models of turbulent magma chambers on ANSYS 5.4 are in good agreement with the expected thicknesses that can be calculated from equation 4.59; see chapter 7 of Harrison (1998). This is a good indication that the finite element method employed by ANSYS is yielding sensible results for turbulent magma convection.

Chapter 5

Finite element methods

5.1 Introduction to finite element methods

The application of the finite element method to an arbitrary partial differential equation in ϕ say, leads to a set of algebraic equations in which there is a finite number of unknowns ϕ_n, at selected points in the domain for the problem. These unknowns are the values of the function ϕ at the points which are labelled by the subscript n, and are called nodes.

The nodes are used, in a variety of ways, to define discrete volumes which are called finite elements. For example, 4 non-co-linear nodes can be used to define a tetrahedral element. Many other shapes exist and their use depends largely on the geometry of the problem. The function ϕ is defined over an element in terms of the nodal values and basis functions, which are also called interpolation functions. Thus a finite element solution allows the definition of ϕ throughout the problem domain in a piecewise fashion over

the individual elements. The choice of interpolation functions can be made in many ways. In general some variational principle has to be invoked to find the interpolation functions. Since there are many variational principles for a given problem, there are correspondingly many finite element methods, all of which lead to the same approximate solution. These methods can differ in their details, even though they all follow the same basic principles.

The method of finite elements is most easily understood in terms of real applications, each of which contain aspects of the general underlying principles outlined above. A typical example of this is the solution of Laplace's equation,

$$\frac{\partial^2 \phi}{\partial x^2} + \frac{\partial^2 \phi}{\partial y^2} = 0$$

using a weighted residual principle known as Galerkin's method. This method is frequently encountered in introductory literature to finite elements and it is also often referred to in more advanced literature on the same subject.

5.2 Galerkin's method

The first step of Galerkin's method is to define an approximate trial solution $\hat{\phi}(x, y)$, which can be expressed as a series summation

$$\hat{\phi}(x, y) = \sum_{L=1}^{N} \phi_L N_L(x, y) \tag{5.1}$$

where ϕ_L is the value of the function $\phi(x, y)$ at the Lth node. N is the total number of nodes in the problem domain. Thus the trail solution is written as a linear combination of the basis functions $N_L(x, y)$

The next step is to require a total of N conditions that will permit the

evaluation of the N values ϕ_L in equation (5.1). In Galerkin's method these conditions are obtained by demanding that

$$\int\int_D \left(\frac{\partial^2\hat{\phi}}{\partial x^2} + \frac{\partial^2\hat{\phi}}{\partial y^2}\right) N_L(x,y)dxdy = 0 \tag{5.2}$$

where the integration is over the entire domain for the problem, D, and L is an index that runs from 1 to N. Stated in words, Galerkin's method requires that the residuals,

$$\left(\frac{\partial^2\hat{\phi}}{\partial x^2} + \frac{\partial^2\hat{\phi}}{\partial y^2}\right)$$

of the governing equation, weighted by each of the N basis functions be zero when integrated over the entire problem domain. It can be shown that the restriction imposed by Galerkin's method is equivalent to those that would arise from a variational principle, if one exists for the problem under consideration. Since all governing equations cannot always be subjected to a variational principle, Galerkin's method has obvious advantages. It can be used even when no variational principle exists (Wang and Anderson, 1982). Before proceeding further it is necessary to integrate equation (5.2) by parts to recast it in the form

$$\int\int_D \left(\frac{\partial\hat{\phi}}{\partial x}\frac{\partial N_L}{\partial x} + \frac{\partial\hat{\phi}}{\partial y}\frac{\partial N_L}{\partial y}\right) dxdy + \int_\gamma \left(\frac{\partial\hat{\phi}}{\partial x}n_x + \frac{\partial\hat{\phi}}{\partial y}n_y\right) N_L d\sigma = 0 \tag{5.3}$$

Since this procedure reduces the order of differentiation by one, there is now only the requirement that $\hat{\phi}(x,y)$ be continuous up to first order instead of to second order.

Below is an example of the implementation of Galerkin's method using triangular elements over the simple problem domain shown in Figure 5.1.

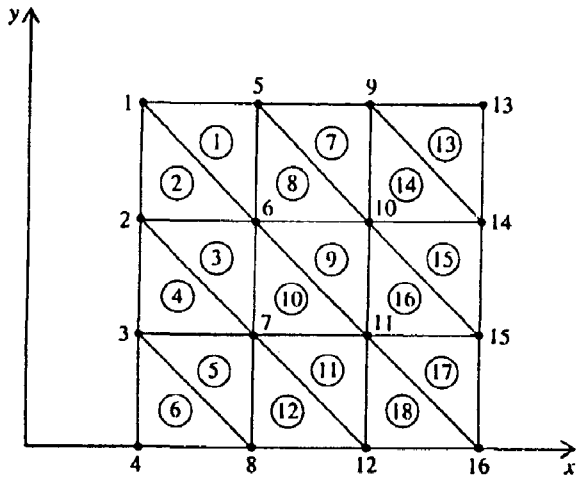

Figure 5.1: The finite element representation of a simple square problem domain. Note that the numbers that are in circles refer to the element numbers while the other numbers refer to the node numbers. From Wang and Anderson (1982).

More details of the elements are shown in Figure 5.2. The trail solution $\hat{\phi}(x, y)$ is defined, throughout the triangular element numbered e, by interpolation of the nodal values of ϕ at the nodes that surround the element e, in this case nodes i, j and m.

Assuming linear interpolation functions for demonstration, it is possible to write, for each element e,

$$\hat{\phi}^e(x, y) = a_0 + a_1 x + a_2 y \tag{5.4}$$

where a_0, a_1 and a_2 are the coefficients that need to be determined from the fact that the given nodal values of $\hat{\phi}$, denoted as h_i, must be recovered at the nodal coordinates, i.e.

$$\begin{aligned} h_i &= a_0 + a_1 x_i + a_2 y_i \\ h_j &= a_0 + a_1 x_j + a_2 y_j \end{aligned}$$

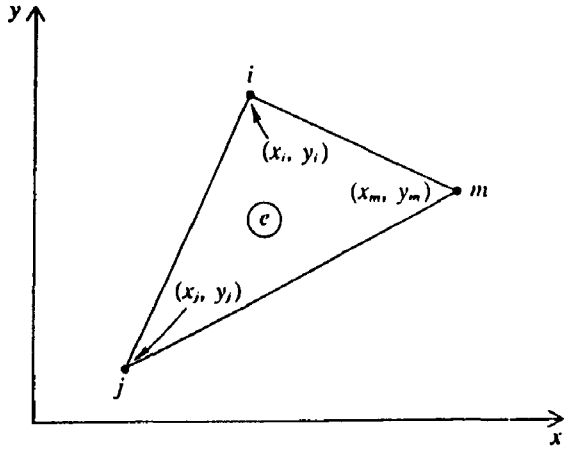

Figure 5.2: The triangular element e has associated nodes i, j and m labelled in counter clockwise order. From Wang and Anderson (1982).

$$h_m = a_0 + a_1 x_m + a_2 y_m$$

If these equations are solved for a_0, a_1 and a_2 and substituted back into equation (5.4), then equation (5.4) can be written as

$$\hat{\phi}^e(x,y) = N_i^e(x,y)h_i + N_j^e(x,y)h_j + N_m^e(x,y)h_m \tag{5.5}$$

where

$$N_i^e(x,y) = \frac{1}{2A^e}[(x_j y_m - x_m y_j) + (y_j - y_m)x + (x_m - x_j)y] \tag{5.6}$$

$$N_j^e(x,y) = \frac{1}{2A^e}[(x_m y_i - x_i y_m) + (y_m - y_i)x + (x_i - x_m)y] \tag{5.7}$$

$$N_m^e(x,y) = \frac{1}{2A^e}[(x_i y_j - x_j y_i) + (y_i - y_j)x + (x_j - x_i)y] \tag{5.8}$$

and

$$2A^e = (x_i y_j - x_j y_i) + (x_m y_i - x_i y_m) + (x_j y_m - x_m y_j) \tag{5.9}$$

The functions $N_i^e(x,y), N_j^e(x,y)$ and $N_m^e(x,y)$ are the element basis functions and A^e is the area of the triangular element, e, shown in Figure 5.2. This procedure is followed for all elements, yielding a system of linear equations to

be solved by well-established procedures. Discussed below is the commercial code that employs similar procedures to calculate convective processes in magma.

5.3 ANSYS 5.4

The commercial code used to obtain the results in the next chapter is called ANSYS. Although this code has many capabilities in areas such as electromagnetism, structural analysis etc., only the fluid dynamical subroutines known as FLOTRAN are used in this thesis. The results obtained in the next chapter were generated on version 5.4. In the following few sections provide a brief explanation of the workings of FLOTRAN 5.4.

5.3.1 Discretization of the governing equations

The continuity, momentum and energy equations of section 4.2 all [1] have the form of equation (5.10), the generic scalar transport equation. There are four types of terms in equation (5.10), respectively, from left to right, the transient, advection, diffusion and source terms.

For the purposes of describing the discretization methods, denote the variable considered, by ϕ. The form of the general scalar transport equation is then

$$\frac{\partial}{\partial t}\left(\rho C_\phi \phi\right) + \partial_i\left(\rho v_i C_\phi \phi\right) = \partial_i\left(\Gamma_\phi \partial_i \phi\right) + S_\phi \qquad (5.10)$$

[1] The turbulent equation, used in turbulent flow calculations, has not been discussed in this thesis. It too has the form of the generic transport equation which is about to be introduced.

Table 5.1: The generic scalar transport equations for the governing equations of an incompressible Newtonian fluid. The meaning of the symbols is explained in chapter 4.

Equation	ϕ	C_ϕ	Γ_ϕ	S_ϕ
Navier-Stokes	v_j	1	μ	$\rho f_j - \partial p/\partial x_j$
Energy	T	h	k	$\Phi + Dp/Dt$
Continuity	1	1	0	

where

$$C_\phi = \text{transient and advection coefficient}$$

$$\Gamma_\phi = \text{diffusion coefficient}$$

$$S_\phi = \text{source terms}$$

Table 5.1 shows what the variables, coefficients, and source terms are for the governing equations. More details on the generic transport equation can be found on pages 7-18 to 7-19 Spencer et al. (1996). Because all the equations have the same form, in what follows, only equation (5.10) is used to illustrate the method by which all the governing equations are solved.

Each of the four types of terms will be outlined in turn. For a complete derivation of the discretization method, consult the detailed expositions on the subjects (White, 1991; Harlow and Amsden, 1971).

The discretization process essentially consists of deriving the element matrices to put together the matrix equation

$$\left(\left[A_e^{\text{transient}}\right] + \left[A_e^{\text{advection}}\right] + \left[A_e^{\text{diffusion}}\right]\right)\{Q_e\} = \left\{S_e^\phi\right\} \qquad (5.11)$$

Galerkin's method of weighted residuals is used here to form the element

integrals. The weighting function for the element will be denoted by W^e. This is also the shape function (Spencer et al., 1997).

Transient term

The first of the element matrix contributions is from the transient term. The general form is simply

$$\left[A_e^{\text{transient}}\right] = \int W^e \frac{\partial(\rho C_\phi \phi)^e}{\partial t} dV \tag{5.12}$$

where dV denotes the volume element of the volume integral. A lumped mass approximation is used so that

$$\int W^e \frac{\partial(\rho C_\phi \phi)}{\partial t} dV = \frac{\partial(\rho C_\phi \phi)}{\partial t} \int W^e dV \tag{5.13}$$

A backward difference scheme is used to evaluate the transient derivative. On a nodal basis, the following implicit formulation is used. The current time step is the n th time step and the expression involves the previous two time step results.

$$\frac{\partial(\rho\phi)}{\partial t} = \frac{(\rho\phi)_{n-2}}{2\Delta t} - \frac{4(\rho\phi)_{n-1}}{2\Delta t} + \frac{3(\rho\phi)_n}{2\Delta t} \tag{5.14}$$

The n th time step produces a contribution to the diagonal of the element matrix, while the derivatives from the previous time step form contributions to the source term.

Advection term

The advection term is handled through a monotone streamline approach based on the idea that pure advection transport is along characteristic lines.

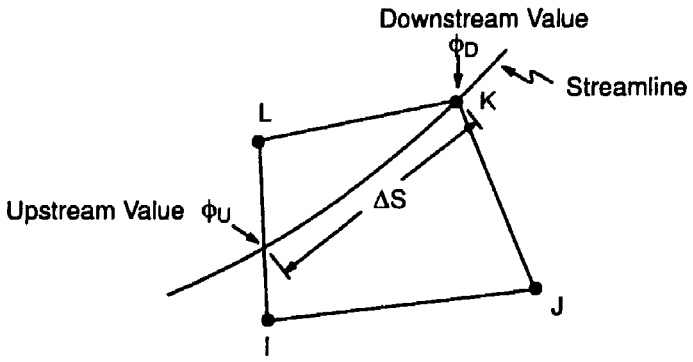

Figure 5.3: The streamline upwind approach. From Spencer et al. (1996).

It is useful to think of the advection transport formulation in terms of a quantity being transported in a known velocity field. See Figure 5.3

The velocity field itself can be visualised as a set of streamlines everywhere tangent to the velocity vectors. The advection terms can therefore be expressed in terms of the streamline velocities.

In pure advection transport, one assumes that all transfer occurs along streamlines. Therefore one may assume that the advection term

$$\frac{\partial}{\partial x^i}\left(\rho v^i C_\phi \phi\right) = \frac{\partial}{\partial s}\left(\rho V_s \phi\right) \tag{5.15}$$

when expressed along a streamline, is constant throughout an element

$$\left[A_e^{\text{advection}}\right] = \frac{d}{ds}\left(\rho V_s \phi\right) \int W^e dV \tag{5.16}$$

This formulation is made for every element, each of which will have only one node which receives contributions from inside the element. The derivative is calculated using a simple difference :

$$\frac{d}{ds}\left(\rho V_s\right) = \frac{\left(\rho V_s \phi\right)_U - \left(\rho V_s \phi\right)_D}{\Delta s} \tag{5.17}$$

where

D = subscript for value at the downstream node

U = subscript for value taken at the location at which the streamline through the downwind node enters the element

Δs = distance from the upstream point to the downstream node

The value at the upstream location is unknown. It can however be expressed in terms of the surrounding unknown nodal values shown in Figure 5.3.

The process consists of cycling through all the elements and identifying the downwind nodes. A calculation is made based on the velocities to see where the streamline through the downwind node came from. Weighting factors are calculated based on the proximity of the upwind location to the neighbouring nodes. Consult Rice and Schnipke (1995) for more details.

Diffusion terms

The expression for the diffusion terms comes from an integration over the problem domain after the multiplication by the weighting function. Denoting volume by V, produces

$$\text{Diffusion contribution} = \int W^e \frac{\partial}{\partial x^i}\left(\Gamma_\phi \frac{\partial \phi}{\partial x_i}\right) dV \tag{5.18}$$

The three terms in the above equation can all be treated in similar fashion. The term in the x direction will thus be used as an illustration.

An integration by parts is applied (Spencer et al., 1997) to get

$$\int W^e \frac{\partial}{\partial x}\left(\Gamma_\phi \frac{\partial \phi}{\partial x}\right) dV = \int \frac{\partial W^e}{\partial x} \Gamma_\phi \frac{\partial \phi}{\partial x} dV \tag{5.19}$$

Once the derivative of ϕ is replaced by the nodal values and the derivatives of the weighting function, the nodal values will be removed from the integrals, i.e. by writing

$$\frac{\partial \phi}{\partial x} = W_x^e \phi \tag{5.20}$$

$$W_x^e = \frac{\partial W^e}{\partial x} \tag{5.21}$$

The diffusion matrix may now be expressed as

$$\left[A_e^{\text{diffusion}}\right] = \int W_k^e \Gamma_\phi W_k^e \, dV \quad \text{(sum over } k = 1, 2, 3) \tag{5.22}$$

Source terms

The evaluation of the source terms consists of multiplying the source terms as depicted in Figure 5.3 by the weighting function and integrating over the volume.

$$S_\phi^e = \int W^e S_\phi \, dV \tag{5.23}$$

5.3.2 Segregated solution algorithm

Each degree of freedom, such as temperature, pressure, the components of velocity etc., is solved in sequential fashion. The equations are coupled, so that each equation is solved with intermediate values of the other degrees of freedom. To see how the respective equations are formed see pages 7-18 to 7-23 in Spencer et al. (1996). The process of solving all these equations in turn and then updating the properties is called a global iteration. The entire global iteration structure is summarised in Table 5.2.

Table 5.2: Outline of the global iteration structure used by the FLOTRAN subroutines.

- Formulate and solve momentum equations approximately then calculate the three velocity values v^i.
- Formulate the pressure equation using the three approximate v^i values from the above step.
- Solve for pressure in the pressure equation
- Update the velocities based on the above velocities and pressure
- Formulate and solve the energy equation for temperature with the new velocities
- Update temperature dependent properties
- Check the rate of change of the solution (Convergence Monitors)
- End of global iteration
- Advance the time step and repeat the procedure

5.4 Fluid solvers

To secure a workable solution, the above algorithm performs repeated sweeps of the matrix equations during every global iteration. In some cases, exact solutions to the equations must be obtained, while in others approximate solutions are adequate. For example, in the solution algorithm of Table 5.2, the time saved by calculating fast approximate solutions to the momentum equations offsets the slightly slower convergence rates one obtains with an exact solution. In the case of the pressure equation, exact solutions are required to ensure conservation of mass. In a thermal problem with constant properties, there is no need to solve the energy equation at all until the flow problem has been converged.

To accommodate the varying accuracy requirements, two types of solvers are provided. Both types of solvers are iterative. The first is a sweeping method known as the Tri-Diagonal Matrix Algorithm (TDMA) and the second consists of semi-direct solvers known as conjugate direction methods. TDMA is used to obtain the approximate solution and the conjugate direction methods are used when exact solutions are needed. The user has control over which method is applied to which degree of freedom.

The TDMA method is an old approach and is described in detail in for example Patankar (1980). This method consists of breaking the problem into a series of tri-diagonal problems where any entries outside the tri-diagonal portion of the matrix are treated as source terms using the previous values. For a completely unstructured mesh, or an arbitrarily numbered system, the method reduces to the Gauss-Seidel iterative method (Elman, 1981). Since it is considered an approximate method, TDMA is repeatedly executed until

it satisfies a preset convergence criterion specified by the user. All the results generated in this thesis have made use of the TDMA method.

Chapter 6

Results from preliminary modelling

6.1 Introduction

This chapter describes three preliminary models of convection in cooling magma chambers. Some results from all three models are included here as examples. Although none of theses results are from models that completely replicate the magmatic environment, they do provide new insights into the geology and formation of real intrusions. They also illustrate the types of results that more advanced models would yield and provide some important information on less complicated systems such as granitic stocks. Future models, envisaged for this project, will be much more complicated than those presented here. For this reason, it is deemed necessary to accumulate a large platform of initial simpler results for comparison to future results that will be obtained from new and more complicated models or refinements based on

some of the existing models.

The models that follow make use of the rhyolitic magma (NRO) discussed in chapter 3. This choice is purely arbitrary as these results are not specific to any particular geological situation. Details of the exact physical properties used for each model can be found in sections 3.2.6, 3.3.1, 3.4.1 and 3.5.1 of chapter 3.

Also provided here, is a brief exposition of the versatility of dimensional scaling as used in the context of the numerical models that follow. For example, the Rayleigh number of the cylindrical chamber of section 6.3 can be defined as

$$Ra = \left(\frac{d}{D}\right) \frac{g\beta\Theta\rho d^3}{\mu k}$$

where the fraction d/D is the aspect ratio of the chamber, D being the diameter of the cylinder. As discussed earlier, in the context of the Rayleigh number for convection between flat horizontal plates, the above Rayleigh number will also decrease as the chamber evolves. Furthermore, any configuration with the same cylindrical geometry and which takes on the same initial Rayleigh number at time $t = 0$, will evolve in a similar fashion to the calculations for the cylindrical model presented here. Similarity allows the calculations for relatively small chambers to be applied to cylindrical magma chambers of any size. As long as the initial Rayleigh number of the model, Ra_m, is the same as that of the larger chamber, the calculations here will apply just as well to the the latter. All that is required is that

$$\frac{Ra_m}{Ra_p} = 1$$

where the subscript p denotes the larger chamber or prototype. In general

the thermal diffusivities and the thermal coefficient of expansion of magmas do not differ much across compositional variations. The implication is that the above similarity condition reduces to

$$\frac{Ra_m}{Ra_p} = \frac{(d_m/D_m)(\Theta_m d_m^3/\mu_m)}{(d_p/D_p)(\Theta_p d_p^3/\mu_p)} = 1$$

For the sake of simplicity in exposition, assume that the prototype chamber has the same aspect ratio as the model. In this case, dynamic similarity is ensured if

$$\frac{(\Theta_m/\mu_m)d_m^3}{(\Theta_p/\mu_p)d_p^3} = 1$$

If we do a calculation with the initial conditions $\Theta_m = 600°C$, $\mu_m = 10^{12}m^2s^{-1}$ and $d_m = 2km$, then the calculations from the model also apply to a prototype chamber with $\Theta_p = 1000°C$, $\mu_p = 10^{10}m^2s^{-1}$ and $d_p = 350m$. This is not an unrealistic situation. The above calculation thus illustrates how dimensional scaling may be employed to apply results from models to real situations. Even though some of the models that follow may at first seem unrealistically small, they could thus still be applicable to a wide class of real magma chambers that have similar geometries to those of the model chambers.

6.2 T-shaped magma chambers

6.2.1 Without the effect of surrounding country rock

The first model is a 2-dimensional model of a T-shaped rhyolitic (NRO) magma chamber. The reason for embracing this geometry is to secure some feel for the cooling evolution of a sill and its possible feeder. This geometry is

also similar to that of the Great Dyke of Zimbabwe which possesses economic mineral deposits. The height of the chamber is 1km. It has been assumed that the magma has an initial temperature of 1400K and that it is emplaced in the chamber which has a fixed wall temperature of 800K. The effect of heat removal by the country rock is not included.

The characteristic cooling time of this chamber is about 3000 years. This is the time taken for the maximum temperature in the chamber to reach a temperature defined by the formula

$$\left(\frac{1}{e}\right)(T_{\text{initial}} - T_{\text{wall}}) + T_{\text{wall}}$$

where $e = 2.7183$. The maximum temperature associated with the cooling time of the T-shaped chamber is, according to the above formula, about 1000K.

Temperature contours for the T-shaped chamber, at various times, are shown in Figures 6.1 and 6.2. These figures show that the two horizontal arms of the chamber cool rapidly in comparison to the central region. This is expected, since the thinner protruding arms clearly have a larger surface-to-volume ratio than the central region of the chamber and thus lose heat to the surrounding country rock more rapidly. Convection in the arms of the chamber only lasts for a small fraction of the total characteristic cooling time [1] since the magma rapidly becomes more viscous with decreasing temperature (see the viscosity in Figure 3.2 of chapter 3). The temperature contours are

[1] It is for this reason that the arms of the chamber are not visible in the lower figures seen in Figure 6.4; as the magma cools and, essentially, solidifies, the velocity vectors in the arms of the chamber attain a zero magnitude and become invisible. The inner part of the chamber is still convecting and the non-zero vectors are thus still visible.

not symmetrical in the initial stages of cooling but become symmetrical later on in the cooling history since convection ceases as the magma becomes more viscous; see Figures 6.1 and 6.2. Clearly, in the final stages of the cooling history of the chamber, heat is conducted out of the chamber while the role of convective heat transport becomes less important. The convection in the initial stage of the cooling history is, however, crucial. It is most likely that differentiation processes within the chamber, such as these described at the beginning of this thesis, would occur as a result of convection, while the melt is still able to flow. It is for this reason that the time intervals have been set to be closely spaced initially and then further apart as the chamber cools: 12, 21, 30, 60, 100, 200, 400, 1200, 1400 and 3000 years. Of particular interest are the details of the initial convection.

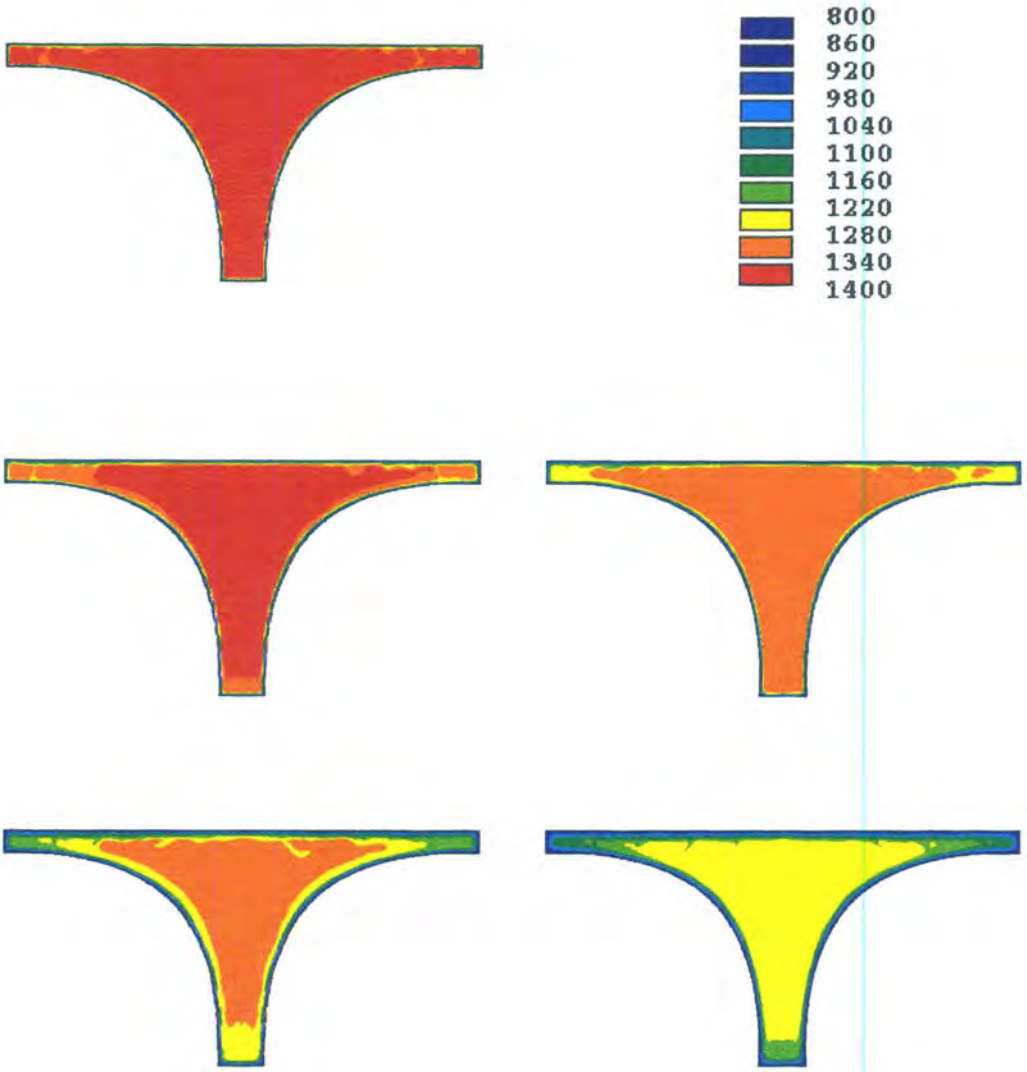

Figure 6.1: Temperature contours, without the effect of country rock, in the T-shaped rhyolitic magma chamber at times 12,21,30,60 and 100 years respectively. An animation of the time evolution of this chamber is included in the compact disc that accompanies this thesis.

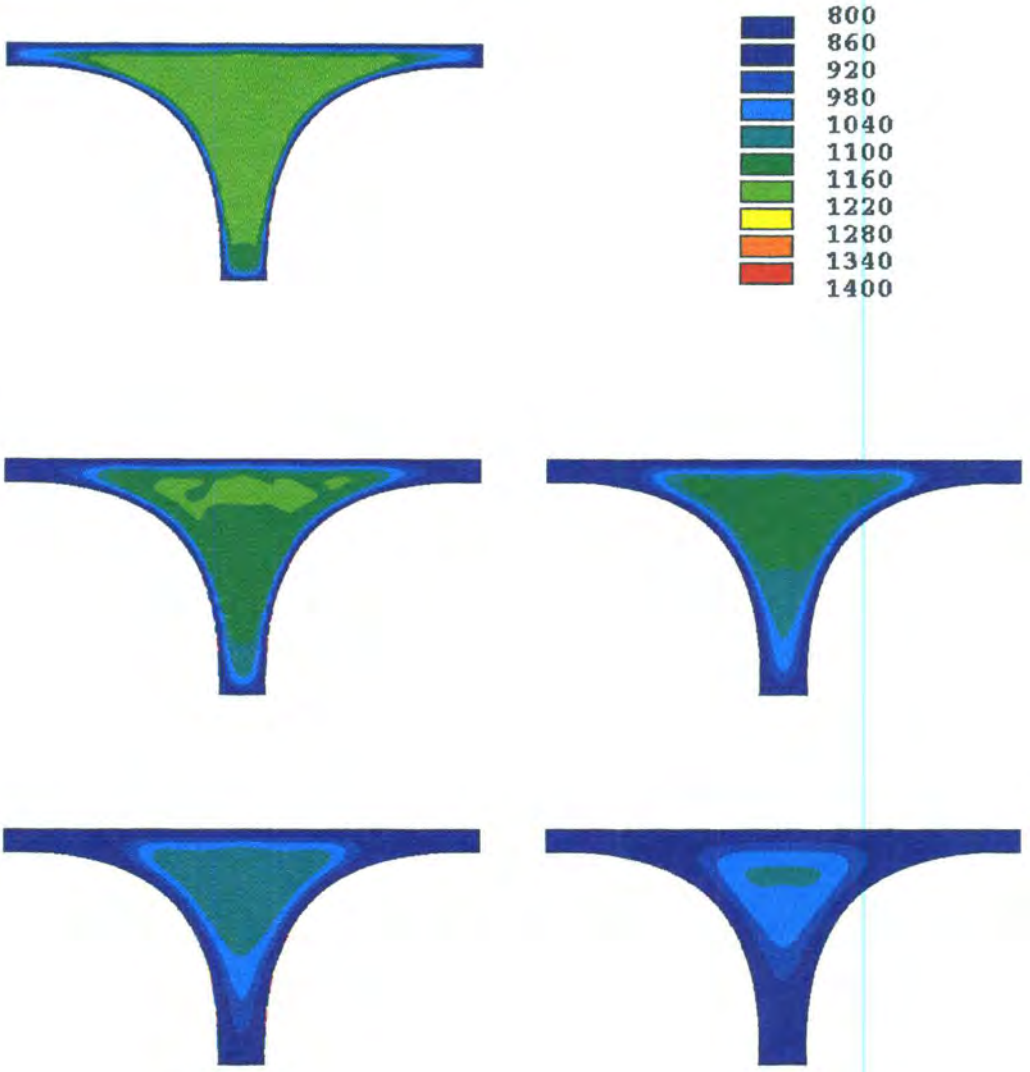

Figure 6.2: Temperature contours, without the effect of country rock, in the T-shaped rhyolitic magma chamber at times 200,400,1200,1400 and 3000 years respectively. An animation of the time evolution of this chamber is included in the compact disc that accompanies this thesis.

6.2.2 With the effect of the surrounding country rock

In the second model the rhyolitic T-shaped chamber is surrounded by solid impermeable country rock. Heat loss to the country rock is modelled purely by conduction using an effective diffusivity to mimic the convective heat loss that would occur as a result of circulating ground water, see section 4.5. The initial temperature of the magma (NRO) is now 1600K and the country rock has an initial surface temperature of 300K with an initial geothermal gradient of 25°C/km. The geothermal gradient is not visible in Figure 6.3 because the contour intervals are too large to resolve such fine detail. Other finer details in the temperature distribution are also lost for this reason but these can, of course, easily be observed by narrowing the contour intervals over a smaller temperature range of interest or simply making more contours. Figure 6.3 shows that the characteristic cooling time of this model, at which the maximum temperature is about 1300K, is much larger than in the previous model; about 10 times more i.e. 30 000 years. The effect of the surrounding country rock is thus to insulate the chamber in comparison to the previous case where the walls are at fixed temperature. This observation was made in similar models which treat the country rock as a porous medium through which ground water is allowed to convect (Harrison, 1998). The present model compares very favourably with a more refined model of exactly the same geometry but surrounded with convecting ground water in porous country rock [2]. The advantage of the more advanced model is that it gives details about the flow regime surrounding the actual chamber. Still, the fact that both models are consistent and were arrived at independently is yet another benchmark which adds more credibility to these calculations.

[2]Personal communication with Mr. Keith Harrison at Rhodes University

Figure 6.4 shows the velocity vectors inside the second T-shaped chamber corresponding to the temperature contours of Figure 6.3. The country rock is included in Figure 6.4 but, because the country rock is treated as a solid, the velocities are zero everywhere outside the T-shaped chamber and are thus not visible. As before, it can be seen that, as the chamber cools, the velocity of the magma in the protruding arms of the chamber becomes essentially zero when the magma solidifies. This is also consistent with the expected high viscosity on the cooler limbs of the chamber as discussed in the previous model.

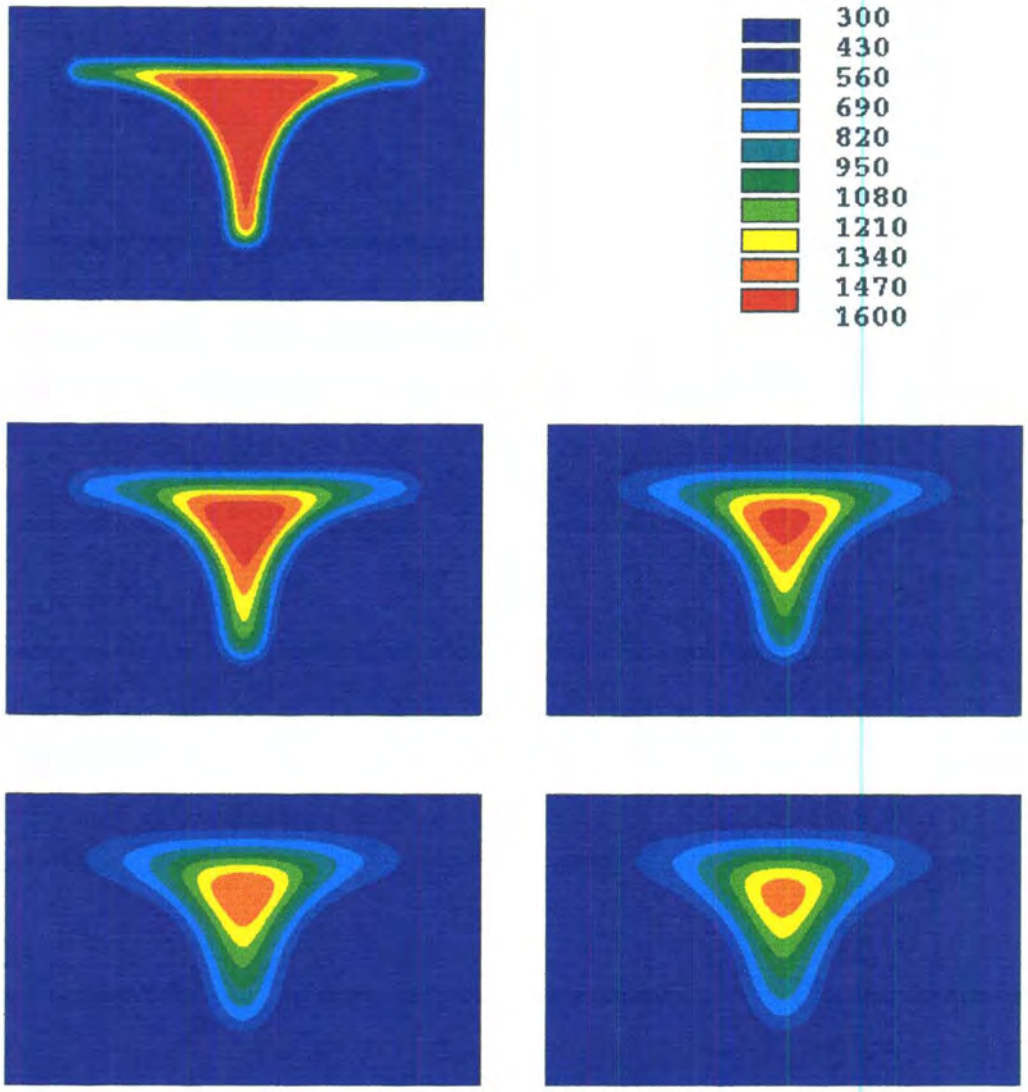

Figure 6.3: Temperature contours in the T-shaped rhyolitic magma chamber surrounded by country rock at times 5,10,15,20 and 25 thousand years respectively.

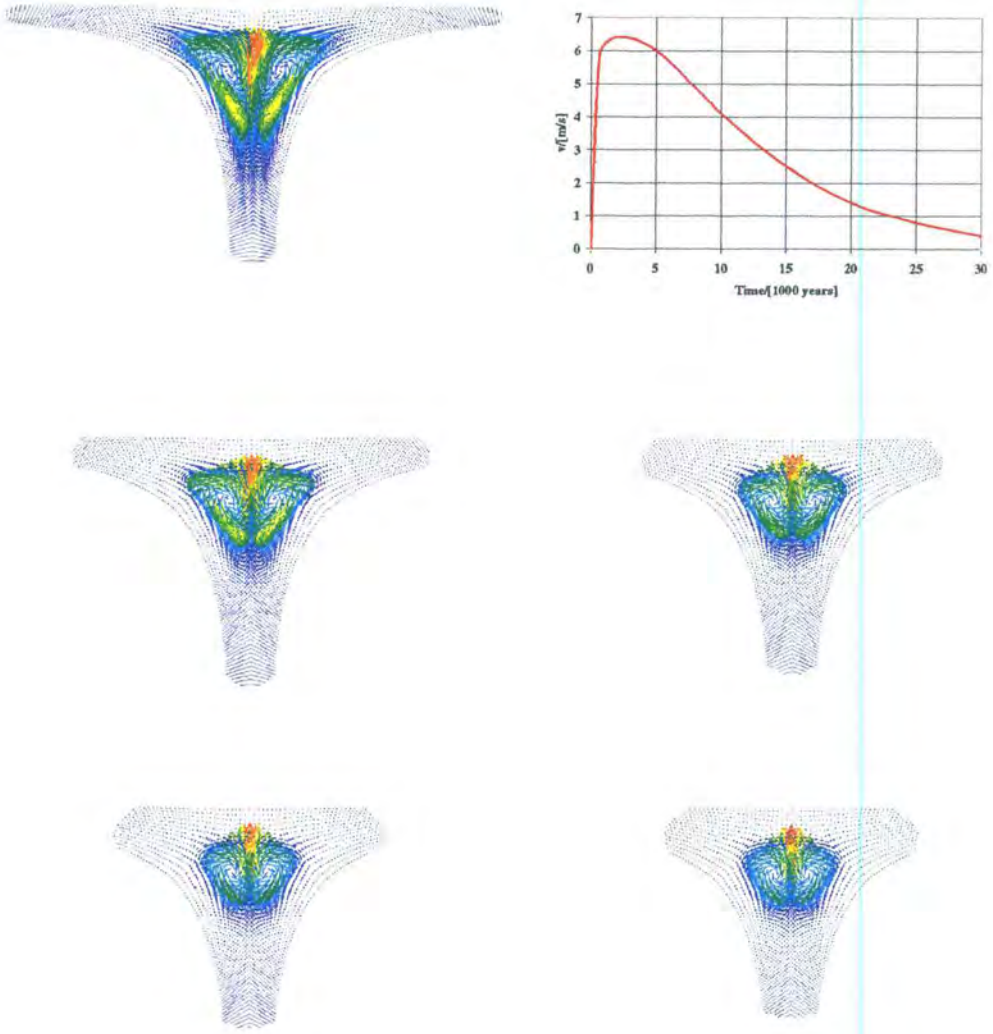

Figure 6.4: Velocity vectors for the T-shaped rhyolitic magma chamber at 5000 year intervals. The maximum velocity that occurs in each of the five figures is colour-coded in red. The solid red line in the graph shows the exact magnitude of the maximum velocities for each time.

6.3 Cylindrical magma chamber

6.3.1 Without the effect of the surrounding country rock

The third model is a 3-dimensional model of a cylindrical magma chamber which initially contains the rhyolitic magma (NRO) at an unusually hot temperature of 1600K. More commonly, rhyolitic magmas in nature, would initially be injected at about 1000°C. Dimensional scaling of the present model, which is only 10 m thick and 50 m across, allows the results presented here to be applied to a chamber of 2 km deep and 10 km across. This model thus makes use of a very important technique called dimensional similitude, a technique which was demonstrated briefly at the beginning of this chapter. It is very important in this type of work and should be considered more seriously in all geological modelling. It has been used for many years in engineering (Rice, 1982).

The walls of the cylindrical chamber are kept at a fixed temperature and the chamber [3] itself is positioned upright so that gravity acts along its length[4].

Figure 6.5 shows some of the elements that are used in the finite element mesh for this problem. As shown in this figure, the element size of this mesh is by necessity not uniform. The arrows indicate regions of the mesh where the elements are most distorted, away from the shape of the outer elements which are regular quadrilaterals with perpendicular sides of roughly equal area. Although there is technically nothing wrong with the elements in these

[3]This chamber is similar to the one shown in Figure 1.1 of the first chapter.

[4]The gravitational acceleration is taken to be 9.81 ms^{-2}.

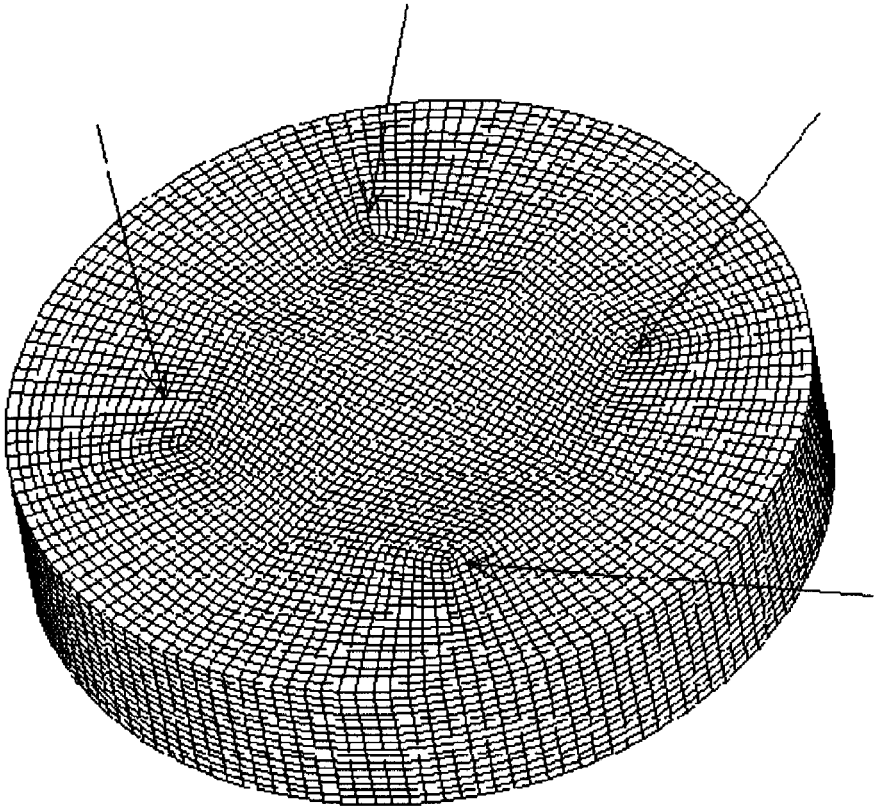

Figure 6.5: The mesh used for the rhyolitic cylindrical magma chamber. The arrows indicate the points at which the mesh is most distorted.

regions [5], the results obtained from this mesh suggest that these regions may provide the instability that is necessary for the onset of convection. This is shown in Figure 6.6 where the 4 regions corresponding to the arrows in Figure 6.5 are where up-welling occurs in the initial stages of the convection. This becomes even more clear in Figure 6.7 and Figure 6.8 which are for the same cylinder after 12 and 18 years respectively. A free mesh of the problem eliminates the symmetry of the original mesh and also the symmetry in the initial phases of the convection. For both meshes though, once the chamber has had time to start convecting rapidly (the magma is initially at rest) the

[5] If the mesh angle (the angle between two sides of an element) is less than 15°, then the preponderance of experience indicates significant errors may occur in the finite element calculations (Spencer et al., 1997).

convective flow patterns are very similar as would be expected.

The results shown here are thus valid since this work, at present, is only interested in the general behaviour of the convecting magma, not specific details of each individual element of fluid. The details of the results for this model do however illustrate a very important point in finite element analysis. Because this is more of academic interest, at present, it is discussed in Appendix E.

In Figure 6.8, a departure from the initial flow pattern, that started at the most distorted elements in the mesh, is observed. The four cells that formed originally (possibly due to the mesh) have developed into two rings of similar cells. The inner ring contains four cells, similar to the original four, and the outer ring now contains 12 new cells at approximately the same radial distance as the original four cells. This type of symmetrical change abounds in a large number of fluid mechanical systems. Coutte flow is possibly the most well know example where such symmetry is observed. Other examples are: Langmuir cells and Bernard hexagonal cells. See Tritton (1977).

Another interesting feature of this model, observed in the temperature contours of Figure 6.9 is the upward shift of the hotter core of the chamber as convection proceeds. This feature is common to all cylindrical models of this type and this fact may have interesting applications in geology (Rice et al., 1998). More refined models, based on real chambers with know geometries (more complicated than cylinders) are presently being constructed on the ANSYS code. Features of these (more realistic) models will definitely yield valuable new insights into the cooling history and solidification processes that occur in magma chambers.

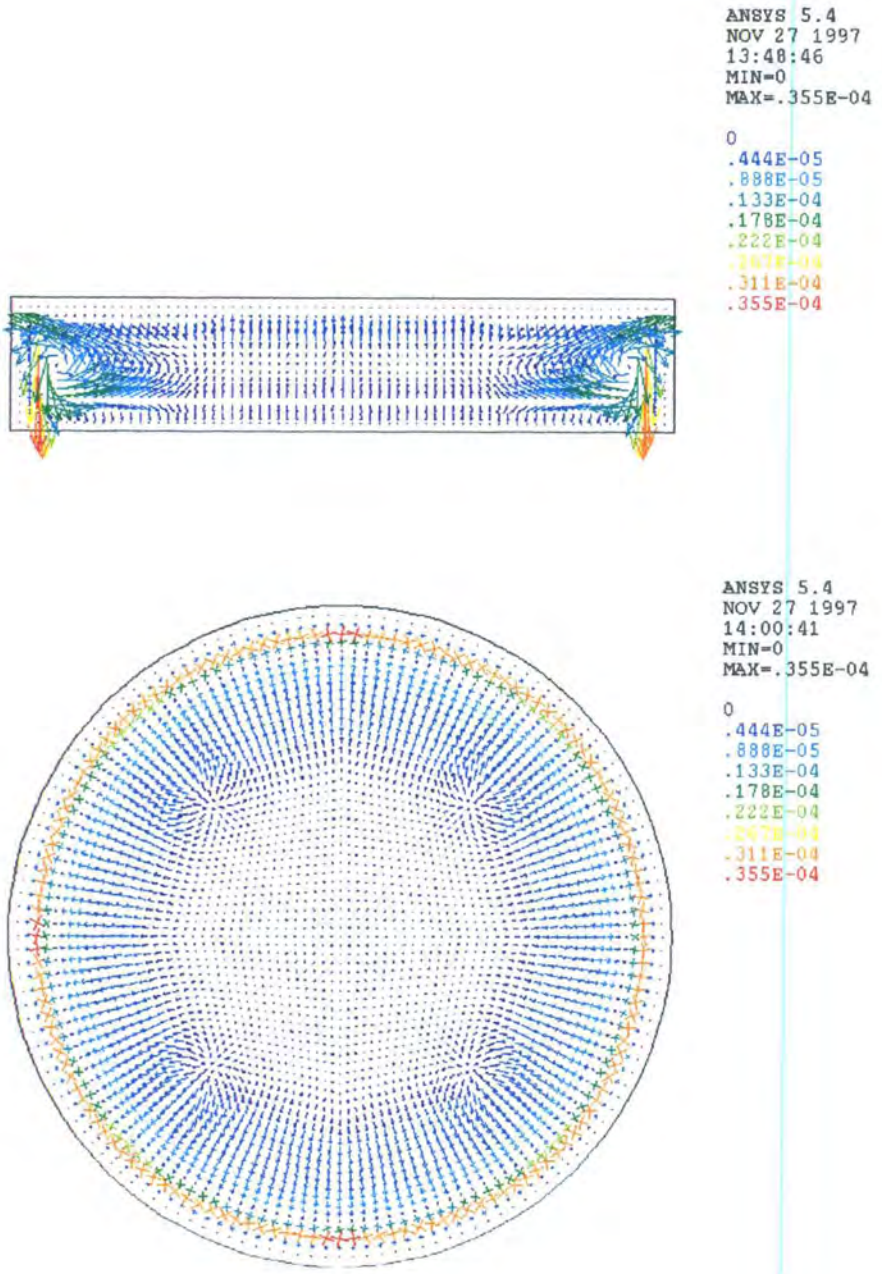

Figure 6.6: Velocity vectors for the rhyolitic cylindrical magma chamber after 8 years. The top figure is a cross-section through the centre of the chamber when it is standing upright with gravity pointing to the foot of this page. The lower figure is an horizontal cross-section through the centre of the cylinder with gravity pointing into the page.

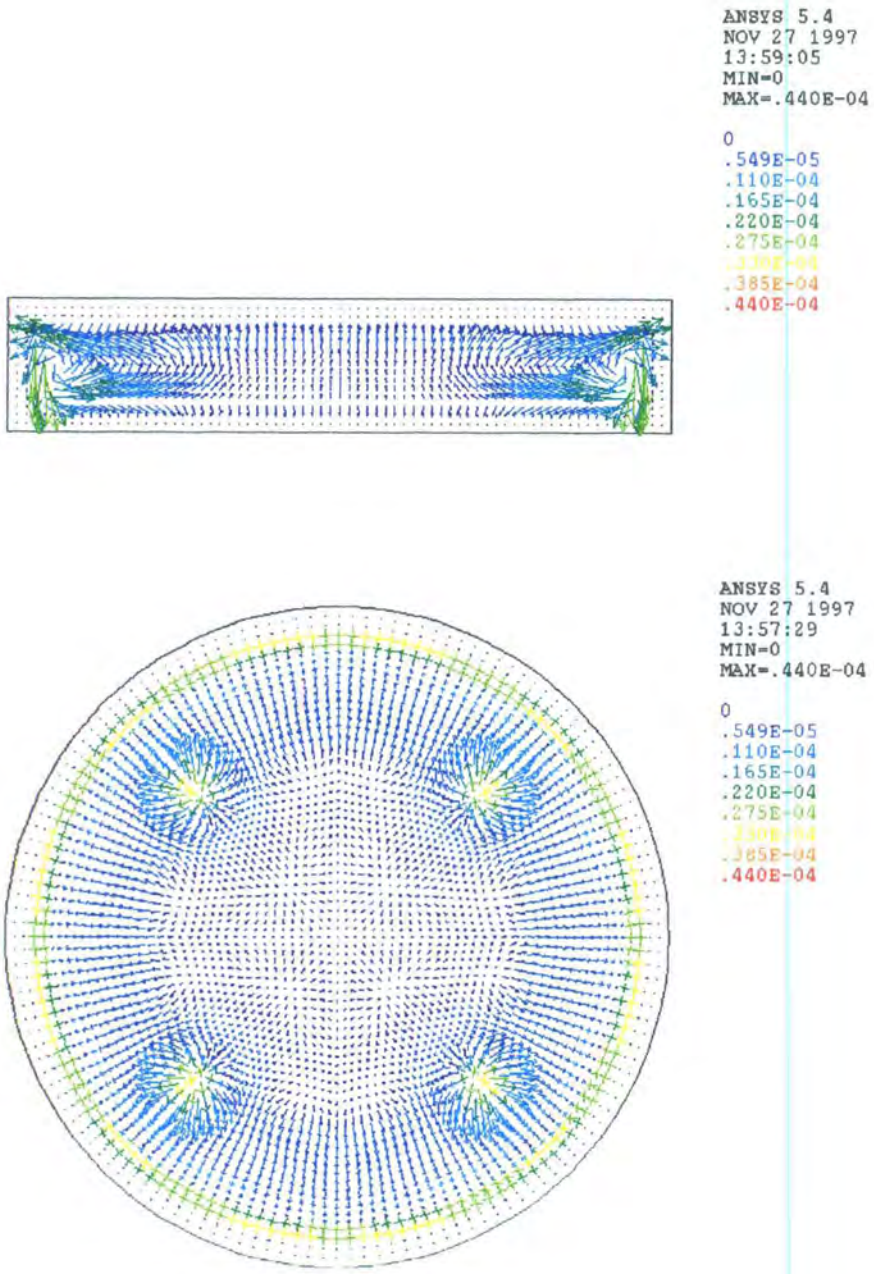

Figure 6.7: Velocity vectors for the rhyolitic cylindrical magma chamber after 12 years. The top figure is a cross-section through the centre of the cylinder when it it standing upright with gravity pointing to the foot of this page. The lower figure is an horizontal cross-section through the centre with gravity pointing into the page.

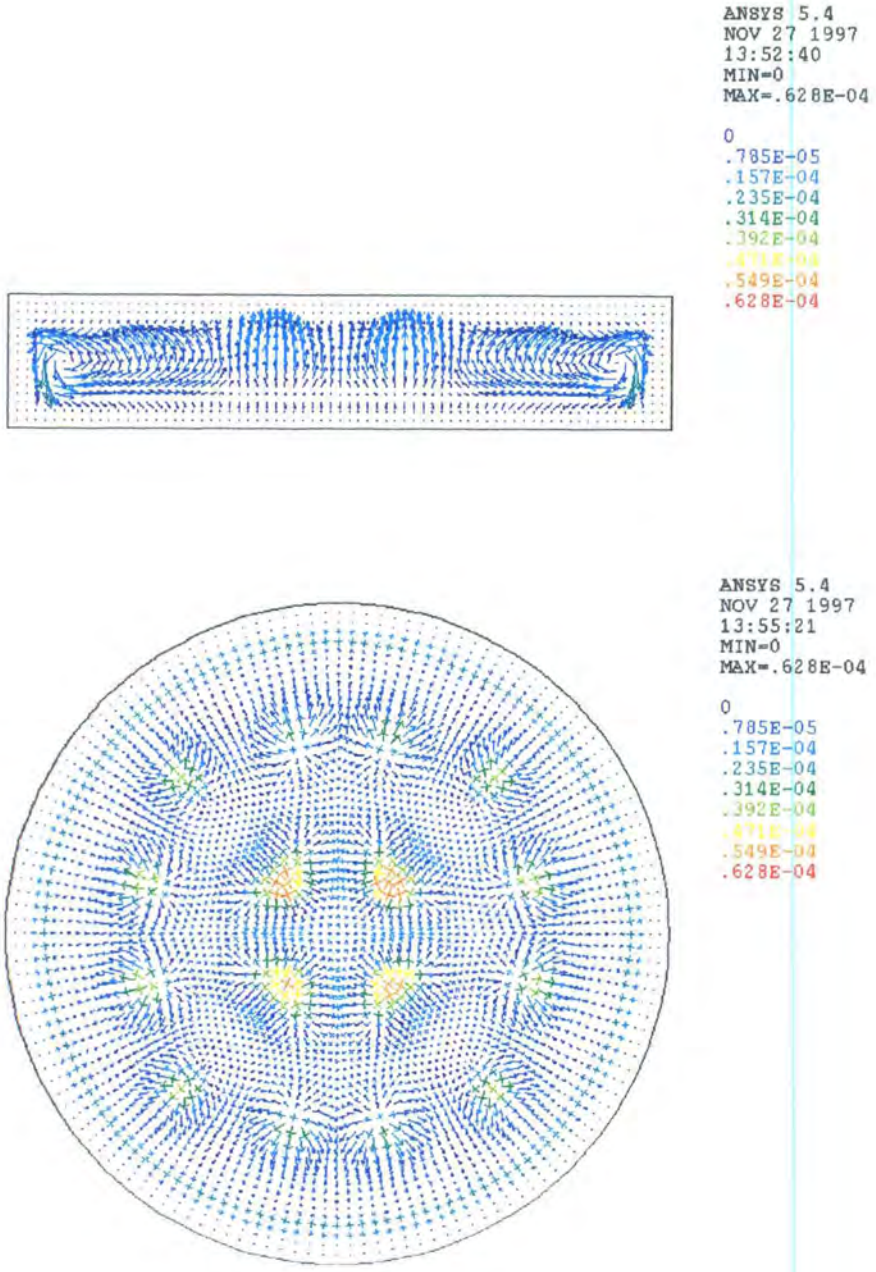

Figure 6.8: Velocity vectors for the rhyolitic cylindrical magma chamber after 18 years. The top figure is a cross-section through the centre of the cylinder when it it standing upright with gravity pointing to the foot of this page. The lower figure is an horizontal cross-section through the centre of the cylinder with gravity pointing into the page.

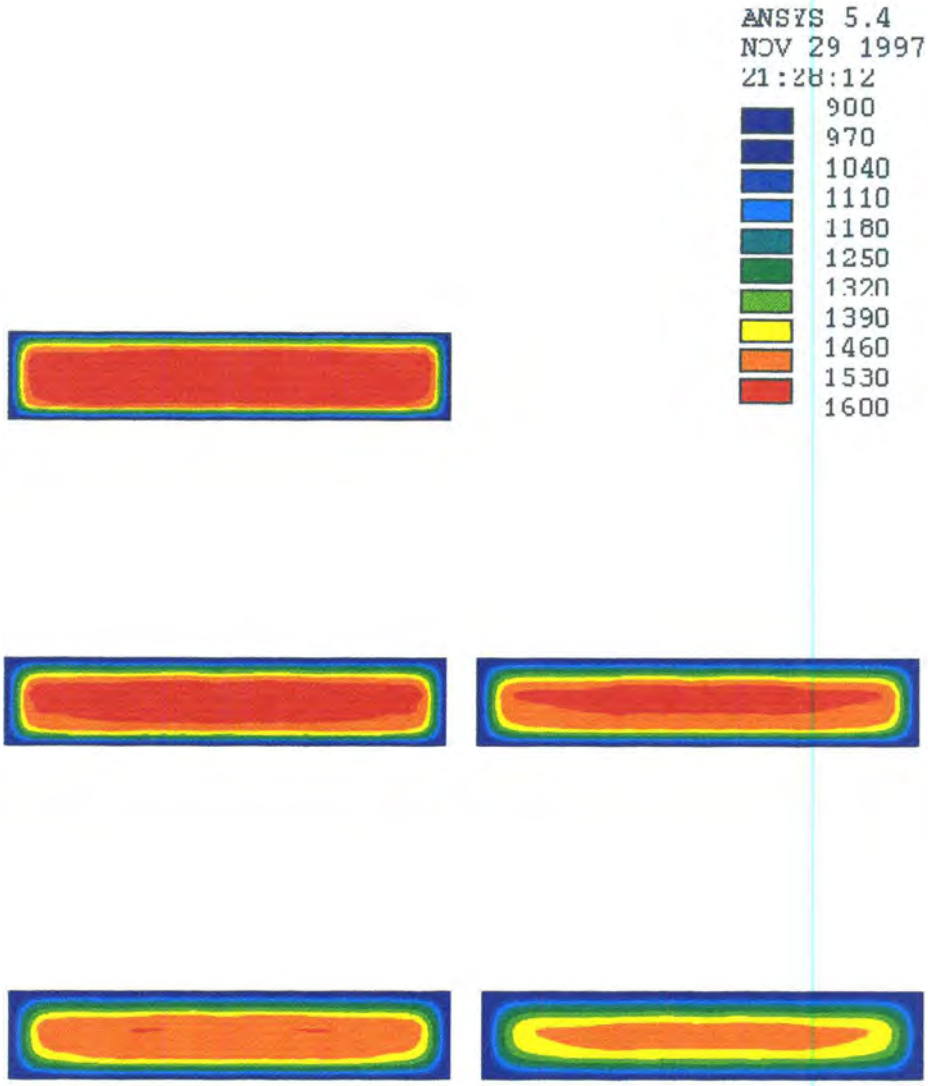

Figure 6.9: Temperature contours for a vertical cross-section of the cylindrical rhyolitic magma chamber for the first 25 years shown at 5 year intervals. The top right hand side cross-section shows that the bulk of the hotter material has shifted to the top half of the chamber.

Chapter 7

Conclusion

7.1 Significance of preliminary results

From the preliminary results and models that are discussed in this thesis it is clear that fulfilment of the main objective of this work requires more advanced computer hardware and more computational time. This is at present the only limiting factor in this work. Even so, the preliminary models that have been devised, taking into account the above limitation, have yielded interesting results which have been met with favourable responses in both the geological and geophysical communities. There follows some features of the initial results presented in this thesis which have immediate application in geology.

The first insight we gained concerns the cooling times of the various magma chambers. These are altered by approximately a factor of four on inclusion of latent heat. In the past it has been very difficult to obtain an accurate ap-

proximation of the cooling time for a given arbitrarily shaped chamber. The models devised so far in this research can provide this information, either by directly modelling the actual chamber, or by modelling a smaller chamber (which is computationally less intensive) and then making use of dynamic similitude to scale the results to that of a real chamber. The cylindrical rhyolitic chamber discussed in chapter 7 is an example of one such model; it is only 10m thick and thus not likely to be of interest in a study of ore-body formation, except if appropriately scaled. Cooling times are essential for many geological models. For example, they give geologists an approximate time scale in which minerals could be deposited by a magma transport process. Flow patterns, such as those shown in the animation of the T-shaped magma chamber (see accompanying compact disc) are equally important.

Another important feature that has been observed is the highly asymmetric rheology of chambers. See for example Figure 1.1 of chapter 1. This feature, at first, might seem physically unintuitive, but when one considers the non-linear nature of the Navier-Stokes equations used in these calculations (specifically the non-linear streaming term which here, unlike most other approaches, has been retained in the calculation), then it is obvious, to someone who is familiar with non-linear systems, that such asymmetry can occur in real situations (Tritton, 1977). Thus, even when a magma chamber is emplaced symmetrically into isotropic surrounding country rock, mineralisation could still take place at some specific preferred location. It is quite possible, according to our calculations, that the orientation of ore bodies surrounding a magma chamber may be a result of the non-linear behaviour of convecting magma (Rice, 1997a). Anisotropic fracture zones or other obviously favourable conditions for ore body formation around the chamber may have formed as a result of the asymmetric behaviour of the convection inside

the magma chamber.

A further innovative feature of the present models is their versatility in displaying the necessary physical information required by geologists. This is illustrated best by the numerous animations on the compact disc accompanying this thesis. This shows, for example, many particle traces, temperature contours and velocity vectors. Arbitrary cross-sections through any part of the chamber can also be made and a fly-through capability, with translucent elements, will soon be available.

Lastly, the models presented here have served as precursors to models which also incorporate the hydrothermal flow in surrounding country rock. Once the effect of circulating hydrothermal groundwater in the surrounding country rock is included, much more interesting behaviour is observed (Harrison, 1998). Nevertheless, the models of this thesis have been useful for comparison to more complex models of this nature. This consistency, of simple models and more complicated models is illustrated by the following few observations that were made during the course of this research.

- chambers with fixed wall temperature generally take longer to cool than equivalent chambers surrounded by purely conducting country rock
- chambers surrounded by convecting ground-water in porous country rock cool much faster (about 10 times) than the above, as the groundwater can remove additional heat from the chamber by convective heat transfer.
- when the country rock is treated as a conducting solid with an appropriately enhanced (effective) conductivity (see section 4.5) then the

chamber is found to cool in approximately the same time as an equivalent chamber surrounded by hydrothermal water in porous country rock.

The above consistency serves as yet another indication (together with other comparisons, such as the known analytic results for a cylinder in terms of the Bessel's function solution of chapter 4) that the numerical results are physically sound. With suitable refinements, real igneous intrusions will soon be modelled and these models will, on the basis of past experience yield profound insights into the problem of ore body formation.

In the final section of this thesis, some of the immediate refinements that are currently being made to models are indicated.

7.2 Future developments

Future models that will be computed on more advanced hardware will be able to be more sophisticated than the preliminary results of this thesis. Some of the immediate refinements that are presently being made are as follows.

- Variable conductivity will be used according to experimental data that is fitted by an appropriate curve fit formula as a function of the magmas temperature and phase.
- All future chambers will (if necessary) take into account the effect of the surrounding porous country rock.
- Phase changes that occur inside the chamber (as the magma solidifies) will be accounted for in terms if enthalpy.

- Specific heats will also be able to vary as necessary, also taking into account a possible phase change.

- The non-Newtonian behaviour of the magma (once it is below its liquidus temperature) will be investigated in an attempt to incorporate better the suspended crystal load presently being dealt with in terms of density (as a function of temperature).

The multidisciplinary nature of this work and also its possibilities for further developments make it one of the fastest growing disciplines in the world (see for example, a search on the world-wide-web using the keywords in the title of this thesis). Academically, this research field has provided the opportunity to learn a variety of skills from fields such as fluid mechanics (both theoretical and experimental), igneous petrology, polymer chemistry, numerical methods (particularly finite element methods) and computer science (data display techniques).

The basic computational and modelling techniques presented in this thesis already show considerable promise for solving some of geology's most perplexing problems, for example, that of obtaining a satisfactory mechanism for the formation of igneous layering and ore body emplacement. It is hoped that this thesis has helped developed a basic groundwork from which further developments in this field can take place.

Appendix A

Glossary of terms appearing in this thesis

This is a glossary of the technical terms which are italicised in the main text. Only the first occurrence of each term is italicised.

Country rock : a rock into which magma intrudes or in which a mineral deposit has been emplaced.

Eutectic systems : a mixture of two or more minerals in definite proportions each of which has crystallised simultaneously from a parent liquid (melt or solution). The temperature at which this simultaneous crystallisation occurs is called the eutectic point.

Igneous rock : rock formed by the solidification of magma.

Igneous intrusions : a body of igneous rock formed by magma which has forced its way (intruded) into surrounding country rock and has subsequently

cooled.

Layering : conspicuously different layers in an igneous intrusion that are due to differences in mineralogical composition, also sometimes called rhythmic layering. See Figure 2.1 chapter 2.

Mafic : from *ma*gnesium and *f*errous iron, applied to rocks that have an abundance of ferromagnesian minerals such as amphiboles, pyroxenes, biotite, garnet, olivine and iron oxides. Mafic rocks are generally dark in colour and heavy.

Magma : a completely or partly molten natural substance, which, on cooling, solidifies as a crystalline or glassy igneous rock.

Mineral deposit : any natural, but locally restricted, concentration of minerals in the Earths crust.

Ore deposit : a mineral deposit in which the minerals concentrated contain substances that are of material significance to people in concentrations that are rich enough to warrant mining.

PGEs : platinum group elements are the metals palladium, osmium, iridium, rhodium, ruthenium and the minerals iridosmine and osmiridium. PGEs are also called platinum group metals (PGMs) or simply platinum metals (PM). They are associated as a group because they are frequently alloyed together and also have similar chemical and physical properties. See page 475 (Bateman, 1950).

Polymer : a substance, usually of high molecular weight, made by linking small molecules into long chain-like structures.

Reserve base : that part of an identified resource that meets the specified minimum physical and chemical criteria related to current mining and production practices, those of grade, quality, thickness and depth. It is the *in situ* demonstrated resource from which reserves are estimated.

Silicic : from silica (SiO_2) or quartz. Igneous rocks with a high free quartz (SiO_2) content are usually referred to as silicic.

Solid-solution series : a series of minerals of identical structure that can contain a mixture of two elements in any ratio. For example, the olivine solid solution series consist of forsterite (Mg_2SiO_4 and fayalite (Fe_2SiO_4).

Appendix B

Contents of attached compact disc

The attached compact disc contains the following displays [1] :

- **anim1.mov** : + square magma chamber and surrounding country rock - temperature contour animation
- **anim2.mov** : + square magma chamber and surrounding country rock - velocity vector animation
- **anim3.mov** : + wedge-shaped magma chamber (country rock not shown), - velocity vector animation

[1] These results were generated by Keith Harrison (indicated by +) and the author (indicated by *) at the Department of Physics and Electronics, Rhodes University, Grahamstown, South Africa. The last movie (anim9.mov) was produced by Soteri Panagou from the Computer Science Department at Rhodes University using data that was produced by the author.

- **anim4.mov** : + wedge-shaped magma chamber - particle trace animation

- **anim5.mov** : * sill-intrusion - velocity vector animation of a T-shaped magma chamber showing "waves"

- **anim6.mov** : * sill-intrusion - velocity vectors of T-shaped magma chamber with conductive country rock, shows freezing of the arms and foot of the chamber

- **anim7.mov** : * 3-dimensional cylinder of aspect ratio 5:1 - velocity vectors of a vertical section through the cylinder

- **anim8.mov** : * 3-dimensional cylinder of aspect ratio 5:1 - velocity vectors of an horizontal section through the cylinder

- **anim9.mov** : visualisation of a crescent-shaped 3-dimensional magma chamber and a real-time rotation of the same chamber, various other 3-dimensional cylinders

Appendix C

Fluid mechanical criteria for crystal settling

In this section a fluid mechanical criteria for estimating the extent to which crystal settling takes place in magma chambers is developed. Use will be made of a curve-fit formula (White, 1991) to calculate the settling velocity. This method does not make use of the well know Stokes law and thus has a slightly broader range of applicability. The Stokes law is only valid for situations in which the Reynolds number is less than or equal to one (White, 1991).

A sufficient condition for the retention of particulate matter in suspension, within a convecting fluid, is that the convective velocities of the fluid exceed the stagnant fluid settling rates (Middleton and Southard, 1985). In what follows, an estimate of typical settling velocities of crystals within a magma chamber will be obtained.

The settling velocity of a solid spherical particle of diameter D and density ρ_s through a fluid of density ρ is given by the curve-fit formula from page 182 of White (1991).

$$\left(\frac{4\rho D}{10\mu}\right) w^3 + \left(\frac{304}{10}\right) w^2 + \left(\frac{72\mu^2 - 4\rho D^3 g\,(\rho_s - \rho)}{3\mu\rho D}\right) w - \frac{4gD(\rho_s - \rho)}{3\rho} = 0 \qquad \text{(C.1)}$$

This equation is accurate to within 10% for all values of $Re \leq 25000$. It is easily solved numerically if the following physical parameters are known:

$$\begin{aligned} \rho_s &= 3300\ \text{kg} \cdot \text{m}^{-3} \quad \text{(density of the crystals)} \\ \rho &= 2580\ \text{kg} \cdot \text{m}^{-3} \quad \text{(density of the magma)} \\ \mu &= 10\ \text{Pa} \cdot \text{s} \quad \text{(viscosity of the magma)} \end{aligned}$$

With the above typical values, the numerical solution of equation (C.1) yields the results shown in Table C.1.

Table C.1: Settling velocities for crystals of various diameters. The values predicted by the curve-fit formula show that a crystal would have to be of diameter 5cm or larger before their settling velocity would exceed the convective velocities that can be expected in the surrounding magma. Primary crystals of such a large size are not observed in mafic rocks.

$w/[\text{m}\cdot\text{s}^{-1}]$	$D/[\text{m}]$
4.204	2.00
2.887	1.00
0.291	0.10
0.003902	0.010
0.00003921	0.0010

From Table C.1 it is clear that, in a typical convecting magma, individual crystals that are likely to form in the magma will not settle; their settling velocities are far less than the estimates for convective velocities. Typically these are at least 10 $cm \cdot s^{-1}$ or higher (Rice, 1995). Crystals would thus have to be at least 5 cm in diameter before they sink faster than they are convected along with the melt. Since primary individual crystals of this size are not observed in the field, it is reasonable to conclude that crystal settling in this typical situation is not possible according to the laws of Physics. Also see Rice and Eales (1995) and section 4.3.

Appendix D

The definition of the Rayleigh number

The Rayleigh number for convection between flat horizontal plates is usually defined as in Table D.1.

It is possible to define a Rayleigh number appropriate to any geometry or convective system that is of interest. For order-of-magnitude calculations however, the present definition is sufficient to characterise the nature of the convection in all sill-like intrusions. The convection could be turbulent, laminar or in some transition region between these extremes. Table D.2 shows the important transition values of the Rayleigh number for convection between flat horizontal surfaces. These values, as well as their applicability to other geometries are discussed further in (Tritton, 1977).

Table D.1: The definition of the Rayleigh number for natural convection between flat horizontal plates.

$$Ra = \frac{g\beta d^3 \rho^2 c_v \Theta}{\mu k}$$

where

g	=	gravitational acceleration
β	=	thermal expansivity
d	=	characteristic dimension
ρ	=	density
k	=	thermal conductivity
c_v	=	specific heat at constant volume
μ	=	viscosity
Θ	=	temperature difference driving the convection

For a typical magma chamber the physical constants could realistically be as follows:

β	=	10^{-5} °C
ρ	=	1000 kg·m^{-3}
Θ	=	200 °C
μ	=	100 Pa·s
k	=	2.0 J·s^{-1}·m^{-1}·K^{-1}
g	=	9.81 m·s^{-2}

Table D.2: Flow characteristics as a function of Rayleigh number for natural convection between flat horizontal plates.

$Ra < 2 \times 10^3$	the fluid does not convect, heat transfer is by conduction only
$Ra < 6 \times 10^4$	the fluid experiences steady, laminar convection only
$Ra > 3 \times 10^6$	the fluid goes over to full turbulent flow (chaotic flow)

$$d = 1000 \text{ m}$$
$$c_v = 1000 \text{ J} \cdot \text{kg}^{-1} \cdot \text{K}^{-1}$$

These values are for the initial stages of the cooling history. The corresponding initial Rayleigh number is calculated to be approximately

$$Ra \approx 10^{14}$$

which corresponds to fully turbulent convection.

Appendix E

Some observations about the onset of convection

In order for a fluid in a finite element analysis of a perfectly symmetrical geometry to convect, there must be some initial instability introduced into the model. In nature, perfectly symmetrical initial conditions do not exist and there is thus always some naturally preferred region where instabilities in buoyancy can initiate the convection. Real convection (possibly as opposed to that which is calculated from the governing equations say) is thus initiated by some initial instability in the buoyancy. Now, if as in theory only, initially there is no preferred region that is more unstable than elsewhere, the fluid will not be able to start convecting. To illustrate this further, a relevant finite element experiment, performed on ANSYS 5.4, will be described next.

The problem of convection between flat horizontal plates is well know in fluid dynamics, see almost any elementary texts on fluid dynamics, for example (Currie, 1993; Lamb, 1916). As already discussed in section 4.3, a linear

instability analysis shows that the onset of convection theoretically occurs at a critical Raleigh number of about 1708 for this situation. When however one solves this problem numerically, one finds that no convection occurs even when the Raleigh number is as high as 10^{15}. If the mesh and time stepping is adequate to secure convergence for the problem, no convection is observed. In fact the more adequate the mesh and the smaller the time stepping, the higher the initial Raleigh number can be, with no convection occurring. These observations are at first quite perplexing since they apparently contradict the instability analysis.

The reason for the above behaviour becomes obvious if one recalls, that in order for convection to occur, there has to be an initial preferred region for the fluid to rise, and in accordance with the conservation of mass, an adjacent region in which fluid may descend. If no such preferred region exist initially, as for example in the above experiment where the mesh and time stepping even precludes the possibility of numerical round off errors, then no convection occurs. It cannot get started. This last assertion is based on the fact that one can introduce an initial preferred region between the flat plates by either (as was possibly the case with the rhyolitic cylinder in chapter 6) using a non uniform mesh, or by introducing a small departure from the usual uniform boundary conditions somewhere on the flat plates. It was found that if one point on the bottom of the plate is initially made slightly hotter that all the other points, then up-welling indeed does occur at this point and convection is subsequently observed as would be expected. The same effect can be obtained by making the mesh non uniform. In this case, convection usually commences in the region where the mesh is most distorted.

Having observed the above, it is worth noting that the observations are of no great consequence to the present numerical models of this project. These only aim at obtaining the general characteristics of the flow regime, not the detailed mechanical solution of each particle of fluid at a given time. The characteristic features of the flow regime in a magma chamber are for the moment more important (as a tool for predicting the location of minerals) than knowing the actual position of the magma at each given time. Even so, the question of how exactly convection should best be initiated is being investigated further. It may become of importance later on in the project when more precise initial conditions of geological units will be used in much more complicated models.

Appendix F

Silicate content of igneous rocks

Table F.1: Main groups of igneous rocks.

Intrusive	**Extrusive**	**Average % SiO_2**
Granite	Rhyolite	72
Granodiorite	Dacite	66
Diorite	Andesite	58
Gabbro	Basalt	50
Peridotite		42

Bibliography

Anderson, D. L. (1987). The depths of mantle reservoirs. In Mysen, B., editor, *Magmatic processes: Physiochemical principles.* The Geochemical Society, Pennsylvania.

Aris, R. (1962). *Vectors, tensors, and the basic equations of fluid mechanics.* Prentice-Hall Inc., New York.

Barnes, H. L. (1979). Solubility of ore minerals. In Barnes, H. L., editor, *Geochemistry of Ore Deposits*, pages 404–460. John Wiley and Sons Inc., New York, second edition.

Bartlett, R. W. (1969). Magma convection, temperature distribution and differentiation. *American Journal of Science*, 267:1067–1082.

Batchelor, G. K. (1967). *An introduction to fluid dynamics.* Cambridge University Press.

Bateman, A. M. (1950). *Economic mineral deposits.* John Wiley and Sons, Inc., New York.

Bird, R. B., Stewart, W. E., and Lightfoot, E. N. (1963). *Transport phenomena.* John Wiley and Sons Inc., New York, third edition.

Botha, A. et al. (1996a). Mathematical modelling of magma. *39th Annual congress of the South African mathematical Society*, 4-6 November, Cape Town.

Botha, A. et al. (1996b). Three dimensional modelling of magmatic convection and crystallisation. *Mineral Exploration*, 24-25 July, Brisbane.

Botha, A. et al. (1997). Mathematical modelling of magma convection. *Proceedings from the 41st Annual Conference of the South African Institute of Physics*, 2-5 July, Pretoria, pg. 73.

Bottinga, Y. and Weill, D. F. (1970). Densities of liquid silicate systems calculated from partial molar volumes of oxide components. *American Journal of Science*, 269:169–182.

Bottinga, Y. and Weill, D. F. (1972). The viscosity of magmatic silicate liquids : a model for calculation. *American Journal of Science*, 272:439–475.

Bowen, N. L. (1915). Crystallisation differentiation in silicate liquids. *American Journal of Science*, 39:175–191.

Brandeis, G. and Jaupart, C. (1986). On the interaction between convection and crystallisation in cooling magma chambers. *Earth and Planetary Science Letters*, 77:345–361.

Campbell, I. H. (1978). Some problems with the cumulus theory. *Lithos*, 11:311–323.

Cann, J. R., Strens, M. R., and Rice, A. (1986). A simple magma-driven thermal balance model for the formation of volcanogenic massive sulphides. *Earth and Planetary Science Letters*, 76:123–134.

Carslaw, H. S. and Jaeger, J. C. (1959). *Conduction of heat in solids.* Oxford University Press, London, second edition.

Chandrasekhar, S. (1957). *Introduction to the study of stellar structure.* Dover Publishers Inc., New York.

Chen, C. F. and Turner, J. S. (1980). Crystallisation in a double-diffusive system. *Journal of Geophysical Research*, 85:2573–2593.

Chorlton, F. (1967). *Textbook of fluid dynamics.* D. Van Nostrand Company Limited, London.

Cox, K. G. and Bell, J. D. (1978). *The interpretation of igneous rocks.* Pergamon Press, Oxford.

Currie, I. G. (1993). *Fundamental fechanics of fluids.* McGraw-Hill International Editions, Toronto.

Darwin, C. (1844). *Geological observations on the volcanic islands, visited during the voyage of H.M.S. Beagle, together with some brief notices on the geology of Australia and the Cape of Good Hope. Being the second part of the voyage of the Beagle , under the command of Capt. Fitzroy, R.N., during the years 1832 to 1836.* Smith Elder, London.

Eales, H. V. et al. (1993). The mafic rocks of the Bushveld Complex: a review of emplacement and crystallisation history, and mineralisation in the light of recent data. *Journal of African Earth Sciences*, 16:1–76.

Elman, H. C. (1981). Preconditioned conjugate-gradient methods for non-symmetric systems of linear equations. In Vichnevetsky, I. V. and Stepleman, R., editors, *Computer methods for partial differential equations*, pages 409–413. IMACS.

Farid, M. et al. (1989). The role of natural convection during melting and solidification of PCM in a vertical cylinder. *Chemical and Engineering Comm.*, 84:43–60.

Gustafson, L. B. (1979). Porphyry copper deposits and calc-alkaline volcanism. In McElhinny, M. W., editor, *The Earth : Its origins, structure and evolution*, pages 427–468. Academic Press Inc., New York.

Hansen, U. (1987). The complex non-linear physics of double-diffusive convection in magma chambers. *Eos Transactions*, 68(44):1536.

Harlow, F. and Amsden, A. (1971). A numerical fluid dynamics calculation method for all flow speeds. *Journal of Computational Physics*, 8.

Harrison, K. (1998). Finite element modelling of magma convection and attendant groundwater flow. *Rhodes University M.Sc. Thesis*, Grahamstown, South Africa.

Harrison, K. et al. (1997). 3-Dimensional calculations of convecting freezing magma chambers and attendant hydrothermal circulation in surrounding country rock. *Proceedings from the American Geophysical Union Fall Meeting*, 8-12 December, San Francisco, California.

Hess, P. C. (1980). Polymerisation model for silicate melts. In Hargraves, R., editor, *Physics of magmatic processes.* Princeton University Press, New Jersey.

Hess, P. C. (1996). South Africa's position in world mineral reserve base. In Botha, E., editor, *Annual report of the Department of Minerals and Energy.* Department of Minerals and Energy, Pretoria.

Hestenes, M. R. and Stiefel, E. (1952). Methods of conjugate gradients for solving linear system. *Journal of Research of the National Bureau of Standards*, 49(6).

Huppert, H. E. et al. (1984). Some effects of viscosity on the dynamics of replenished magma chambers. *J. Geophys. Res.*, 89(B8):6857–6877.

Huppert, H. E., Stephen, R., and Sparks, J. (1982). The fluid dynamics of a basic magma chamber replenished by hot, dense ultra-basic magma. *Contributions to Mineralogy and Petrology*, 75:279–289.

Huppert, H. E. and Turner, J. S. (1991). Comments on 'On convective style and vigour in sheet-like magma chambers' by Bruce D. Marsh. *Journal of Petrology*, 32:851–854.

Kreith, F. and Bohn, M. S. (1993). *Principles of heat transfer.* West Publishing Company, St. Paul, fifth edition.

Lamb, H. (1916). *Hydrodynamics.* Cambridge University Press, Cambridge, fourth edition.

Maaloe, S. (1985). *Principles of igneous petrology.* Springer-Verlag, Berlin.

Marsh, B. D. (1989). On convective style and vigour in sheet-like magma chambers. *Journal of Petrology*, 30:479–530.

Martin, D. (1989). A stirring tale of crystals and currents. *New Scientist*, 1692:53–59.

Martin, D., Griffiths, R. W., and Campbell, I. H. (1987). Compositional and thermal convection in magma chambers. *Contributions to Mineralogy and Petrology*, 96:465–475.

McBirney, A. R. and Murase, T. (1984). Rheological properties of magmas. *Annual Review of Earth and Planetary Science*, 12:337–357.

McBirney, A. R. and Nicolas, A. (1997). The skaergaard layered series. Part II: magmatic flow and dynamic layering. *Journal of Petrology*, 38(5):569–580.

McBirney, A. R. and Noyes, R. (1979). Crystallisation and layering of the Skaergaard intrusion. *Journal of petrology*, 20:487–554.

McCarthy, R. G. et al. (1985). Mineral layering in the Bushveld Complex: Implications of Cr abundances in magnetite from closely spaced magnetitite and intervening silicate-rich layers. *Economic Geology*, 80:1062–1074.

Middleton, G. V. and Southard, J. B. (1985). Mechanics of sediment movement. *Society of Economic Paleontologists and Mineralogists (Eastern Section)*, page 297.

Murase, T. and McBirney, A. R. (1973). Properties of some common igneous rock and their melts at high temperatures. *Geological Society of America Bulletin*, 84:3563–3592.

Patankar, S. V. (1980). *Numerical heat transfer and fluid flow.* Hemisphere, New York.

Pinder, G. F. and Gray, W. G. (1977). *Finite element simulation in surface and subsurface hydrology.* Academic Press Inc., New York.

Reid, J. K. (1971). On the methods of conjugate gradients for the solution of large sparse sets of linear equations. In Reid, J. K., editor, *Proceedings of the conference on large sparse sets of linear equations*, pages 231–254. Academic Press.

Rice, A. (1981). Convective fractionation; a mechanism to provide cryptic zoning (microsegregation), layering, crescumulates, banded tuffs and explosive volcanism in igneous processes. *Journal of Geophysical Research*, 86(1):405–417.

Rice, A. (1982). Scaling problems in double diffusive experiments attempting to replicate magma chambers. *Eos Transactions*, 63(45):1130.

Rice, A. (1993). Dynamics of magma chambers. In Stone, D. and Runcorn, S., editors, *NATO Proceedings on Geophysical Fluid Dynamics*, pages 287–306. Kluwer Press, Amsterdam.

Rice, A. (1995). Are stringers a manifestation of solute banding? *Mineralogy and Petrology*, 54:137–147.

Rice, A. (1997a). A means to secure the Bushveld Complex in a single pulse. *Proceedings from the fall meeting of the American Geophysical Union*, December, San Francisco, California.

Rice, A. (1997b). A model for PGE enrichment due to the splitting of freezing magma chambers by suspended crystal loads. *Exploration and Mining Geology*, 6:129–137.

Rice, A. and Eales, H. V. (1995). The Densities of Bushveld Melts: textural and hydrodynamic criteria. *Mineralogy and Petrology*, 54:45–53.

Rice, A. et al. (1998). Solidifying magma chambers and the mobilisation of hydrothermal circulation in country rock. *SACAM 98*, 12-14 January, Cape Town.

Rice, A. and von Gruenewaldt, G. (1994). Convective scavenging and cascade enrichment in Bushveld Complex melts: possible mechanism for

concentration of platinum-group elements and chromite in mineralised layers. *Trans. Instn. Min. Metall.*, 103:B31–B38.

Rice, A. and von Gruenewaldt, G. (1995). Shear aggregation (convective scavenging) and cascade enrichment of PGEs and chromite in mineralised layers of large layered intrusions. *Mineralogy and Petrology*, 54:105–117.

Rice, J. G. and Schnipke, R. J. (1985). A monotone streamline upwind finite element method for convection-dominated flows. *Computer Methods in Applied Mechanics and Engineering*, 48:313–327.

Rudman, M. (1992). Two-phase natural convection: implications for crystal settling in magma chambers. *Physics of the Earth and Planetary Interiors*, 72:153–172.

Rudman, M. (1996). One-field equations for two-phase flows. *Journal of the Australian Mathematical Society*, 90:167–189.

Schowalter, W. R. (1978). *Mechanics of non-Newtonian fluids.* Pergamon Press, Oxford, first edition.

Sharpe, M. R. (1985). Strontium isotope evidence for preserved density stratification in the main zone of the Bushveld Complex, South Africa. *Nature*, 316:119–126.

Shaw, H. R. (1965). Comments on viscosity, crystal settling and convection in granitic magmas. *American Journal of Science*, 263:120–152.

Snyder, D., Gier, E., and Carmichael, I. (1994). Experimental determination of the thermal conductivity of molten $CaMgSi_2O_6$ and the transport of

heat through magmas. *Journal of Geophysical Research*, 99(B8):15,503–15,516.

Sparks, R. S. J. and Huppert, H. E. (1984). Density changes during the fractional crystallisation of basaltic magmas: fluid dynamic implications. *Contributions to Mineralogy and Petrology*, 85:300–309.

Spencer, E. et al. (1997). Ansys theory reference manual. In Kohnke, P., editor, *ANSYS Release 5.4*. Swanson Analysis Systems Inc., Houston.

Spera, F., Yuen, D., and Kirschvink, S. J. (1982). Thermal boundary layer convection in silicic magma chambers : Effects of temperature-dependent rheology and implications for thermo-gravitational chemical fractionation. *Journal of Geophysical Research*, 87(B10):8755–8767.

Tritton, D. J. (1977). *Physical fluid dynamics.* Van Nostrand Reingold, London.

Turner, J. S. (1973). *Buoyancy effects in fluids.* Cambridge University Press, London.

Turner, J. S. (1980). A fluid-dynamical model of differentiation and layering in magma chambers. *Nature*, 285:213–215.

Vlack, L. H. V. (1964). *Elements of material science.* Addison-Wesley Publishing Company, London, second edition.

Wager, L. and Brown, G. (1967). *Layered igneous rocks.* Oliver and Boyd, Edinburgh.

Wang, F. M. and Anderson, M. P. (1982). *Introduction to Groundwater Modeling: Finite difference and finite element methods.* W.H. Freeman and Company, San Francisco.

Weinstein, S. A., Yuen, D. A., and Olson, P. L. (1988). Evolution of crystal settling in magma-chamber convection. *Earth and planetary science letters*, 87:237–248.

White, F. M. (1991). *Viscous Fluid Flow.* McGraw-Hill, New York, second edition.

Williams, H. and McBirney, A. R. (1979). *Volcanology.* Freeman, Cooper and Company, San Francisco.